Precursors and Pathways Leading to Enhanced Secondary Organic Aerosol Formation during Severe Haze Episodes

Zheng, Yan

2021-12-07

Zheng , Y , Chen , Q , Cheng , X , Mohr , C , Cai , J , Huang , W , Shrivastava , M , Ye , P , Fu , P , Shi , X , Ge , Y , Liao , K , Miao , R , Qiu , X , Koenig , T K & Chen , S 2021 , ' Precursors and Pathways Leading to Enhanced Secondary Organic Aerosol Formation during Severe Haze Episodes ' , Environmental Science and Technology , vol. 55 , no. 23 , pp. 15680-15693 . https://doi.org/10.1021/acs.est.1c04255

http://hdl.handle.net/10138/352102
https://doi.org/10.1021/acs.est.1c04255

unspecified
acceptedVersion

Precursors and pathways leading to enhanced secondary organic aerosol formation during severe haze episodes

Yan Zheng[1], Qi Chen[1,*], Xi Cheng[1], Claudia Mohr[2], Jing Cai[3], Wei Huang[3], Manish Shrivastava[4], Penglin Ye[5], Pingqing Fu[6], Xiaodi Shi[1], Yanli Ge[1], Keren Liao[1], Ruqian Miao[1], Xinghua Qiu[1], Theodore K. Koenig[1], Shiyi Chen[1]

[1]State Key Joint Laboratory of Environmental Simulation and Pollution Control, BIC-ESAT and IJRC, College of Environmental Sciences and Engineering, Peking University, Beijing 100871, China

[2]Department of Environmental Science and Analytical Chemistry, Stockholm University, Stockholm 11418, Sweden

[3]Institute for Atmospheric and Earth System Research, Faculty of Science, University of Helsinki, Helsinki 00014, Finland

[4]Pacific Northwest National Laboratory, Richland, Washington 99352, USA

[5]Shanghai Key Laboratory of Atmospheric Particle Pollution and Prevention, Department of Environmental Science and Engineering, Fudan University, Shanghai 200433, China

[6]Institute of Surface-Earth System Science, Tianjin University, Tianjin 300072, China

[*]*Correspondence to*: Qi Chen (qichenpku@pku.edu.cn)

TOC art

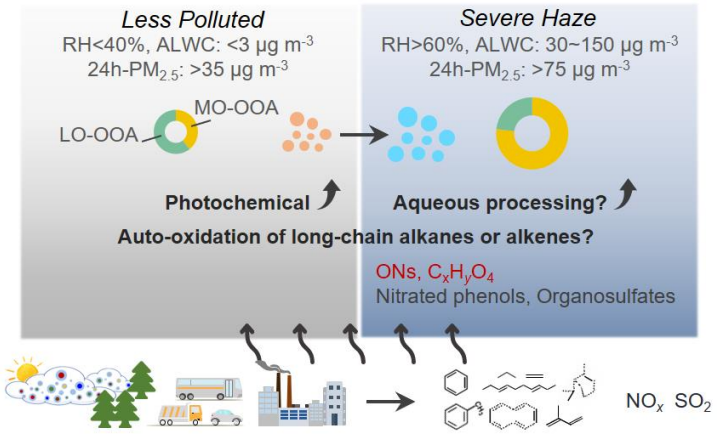
Less Polluted
RH<40%, ALWC: <3 μg m-3
24h-PM2.5: >35 μg m-3
Severe Haze
RH>60%, ALWC: 30~150 μg m-3
24h-PM2.5: >75 μg m-3
MO-OOA
LO-OOA
Photochemical
Aqueous processing?
Auto-oxidation of long-chain alkanes or alkenes?
ONs, CxHyO4
Nitrated phenols, Organosulfates
NOx SO2

Abstract

Molecular analyses help to investigate the key precursors and chemical processes of secondary organic aerosol (SOA) formation. We obtained the sources and molecular compositions of organic aerosol in $PM_{2.5}$ in winter in Beijing by online and offline mass spectrometer measurements. Photochemical and aqueous processing were both involved in producing SOA during the haze events. Aromatics, isoprene, long-chain alkanes or alkenes, and carbonyls such as glyoxal and methylglyoxal were all important precursors. The enhanced SOA formation during the severe haze event was predominantly contributed by aqueous processing that was promoted by elevated amounts of aerosol water, for which multifunctional organic nitrates contributed most, followed by organic compounds having 4 oxygen atoms in their formulae. The latter included dicarboxylic acids and various oxidation products from isoprene and aromatics as well as products or oligomers from methylglyoxal aqueous uptake. Nitrated phenols, organosulfates, and methanesulfonic acid were also important SOA products but their contributions to the elevated SOA mass during the severe haze event were minor. Our results highlight the importance of reducing nitrogen oxides and nitrate for future SOA control. Additionally, the formation of highly oxygenated long-chain molecules with low degree of unsaturation in polluted urban environments requires further research.

Keywords

SOA, molecular composition, haze, aqueous processing, dicarboxylic acid, organic nitrates

Synopsis

This research investigates the various precursors and formation pathways of SOA in polluted urban environments.

1 Introduction

Rapid economic development and modernization in China has led to severe air pollution.[1] The densely populated Northern China Plain (NCP) is one of the most polluted areas in China where the concentrations of particles with an aerodynamic diameter less than 2.5 μm ($PM_{2.5}$) may reach up to several hundreds of μg m^{-3} during the winter-haze episodes.[1] Secondary aerosol formation plays an important role in the haze development.[2] Despite of effective reductions of the sulphur dioxide (SO_2) and reactive oxides of nitrogen (NO_x) emissions in the past ten years, the mass concentrations of secondary organic aerosol (SOA) in $PM_{2.5}$ remain high in the NCP.[3-5]

The high hydroxyl radical oxidation rates in the NCP in winter would produce significant amounts of secondary organic precursors to form SOA through different pathways.[6] Several oxygenated organic aerosol (OOA) factors have been identified by the positive matrix factorization (PMF) analysis of aerosol mass spectrometer (AMS) and aerosol chemical speciation monitor (ACSM) data.[7-10] Both of the photochemical and aqueous pathways are involved in the SOA formation.[7, 11] In particular, high concentrations of inorganic salts as well as organic components lead to high aerosol liquid water content (ALWC) when relative humidity (RH) becomes high (e.g., above 60% in winter in Beijing).[12] Water-soluble oxygenated organic compounds dissolve into aerosol water and may undergo further aqueous reactions to form SOA.[13, 14] Enhanced SOA production by aqueous processing has been found in the United States and Europe.[15, 16] In the NCP, positive correlations of the SOA mass concentrations with RH or ALWC have been observed in winter.[7, 11] Elevated mass concentrations of some OOA factors during the humid-haze events have been attributed to aqueous processing that may include heterogeneous or condensed-phase reactions under dark or photochemical conditions.[17, 18] Recent results from the extractive electrospray ionization time-of-flight mass spectrometer (EESI-TOF-MS) show strong compositional variability of organic aerosol (OA) during the haze events in NCP,[18] highlighting the complexity of SOA formation in polluted environments. However, the lack of molecular information of OA hinders the understanding of key precursors and the contributions of various pathways. Moreover, NO_x are expected to affect the SOA formation directly through forming nitrogen-containing compounds or indirectly through altering the oxidant concentrations in polluted environments.[19] The formation mechanisms of nitrogen-containing organic species remain largely unknown.[20]

In this study, we deployed a time-of-flight ACSM (TOF-ACSM) and a long time-of-flight AMS (LTOF-AMS) to measure the chemical compositions of $PM_{2.5}$ and submicron particles (PM_1) in winter of 2017 in Beijing. The PMF analysis was conducted for these online data sets to identify the OA sources. We also conducted offline molecular analysis for the OA composition of $PM_{2.5}$ deposited on Teflon filters by using an iodide-adduct time-of-flight chemical ionization mass spectrometer (I^--TOF-CIMS) coupled with a filter inlet for gases and aerosols (FIGAERO). The molecular composition was investigated together with the PMF source apportionment of OA to understand the key precursors and processes that lead to the enhanced SOA production during severe haze episodes.

2 Experimental methods

2.1 Online measurements

Measurements were conducted during 16 December 2017 to 10 January 2018 at the roof site on an eighth-floor building in the campus of Peking University that represents a typical urban environment.[21] The $PM_{2.5}$ mass concentrations were measured by a Thermo Scientific tapered element oscillating microbalance monitor (TEOM 1400A, heated to 30°C). The chemical compositions of non-refractory (NR-) $PM_{2.5}$ and PM_1 were measured by the Aerodyne TOF-ACSM and LTOF-AMS. Trace gases such as carbon monoxide (CO), NO_x, SO_2, and ozone (O_3) were measured by a series of Thermo Scientific analyzers (48i-TL, 42i-TL, 43i-TL, and 49i-TL, respectively). Meteorological parameters, including temperature (T), RH, wind speed (WS) and wind direction (WD), were measured by a Met One weather station (083E, 092, and 020C, respectively). All data reported here refer to the local time in Beijing (UTC+8).

The TOF-ACSM was equipped with a $PM_{2.5}$ aerodynamic lens and a capture vaporizer (CV). A cyclone (URG, 2000-30EHB) was installed in front of the sampling inlet to remove coarse particles. The TOF-ACSM switched between $PM_{2.5}$ and PM_1 sampling every half an hour by changing the sampling flowrate through the cyclone. For the $PM_{2.5}$ measurements, a flow rate of 4.8 L min^{-1} was set to achieve a size cut of about 3 μm at the cyclone and then the aerodynamic lens in TOF-ACSM set the measurement domain to < 2.5 μm. For the PM_1 measurements, a flow rate of 16.7 L min^{-1} was set to achieve a size cut of about 1 μm at the cyclone and these submicron particles shall pass through the $PM_{2.5}$ aerodynamic lens. The LTOF-AMS was equipped with a PM_1 aerodynamic lens and a standard vaporizer and sampled the air from a separate inlet. The inlet RH was between 12 and 45% during the campaign for both of the TOF-ACSM and AMS.

The TOF-ACSM data had a 2-min time resolution and were processed in Tofware (Tofwerk version 2.5.13). The ionization efficiency (IE) and relative IE (RIE) were calibrated following the standard procedures by using 300-350 nm pure NH_4NO_3 and $(NH_4)_2SO_4$.[22] The RIE values applied for nitrate, sulfate, ammonium, chloride, and OA were 1.05, 1.6, 3.7, 1.3, and 1.4, respectively. The CV TOF-ACSM has a collection efficiency (CE) of ~1, which has been verified in our previous work.[23] Agreements between the TOF-ACSM and the TEOM data for $PM_{2.5}$ mass concentrations are shown in Figure S1 in the Supporting Information (SI). To identify the OA sources, the PMF analysis for $PM_{2.5}$ was performed on the unit-mass organic mass spectra between mass-to-charge ratio (*m*/*z*) 12 and 200 by using the Igor PMF evaluation tool (PET, version 3.00B).[8, 24] Details of the solution selection are provided in Sect. A of the SI. The component mass concentrations and OA source apportionment for PM_1 were compared in detail previously, and the results of the TOF-ACSM and LTOF-AMS agreed with each other except some differences in the mass loadings of chloride and OA factors.[23] The number and mass spectra of the statistical factors for $PM_{2.5}$ were similar to those for PM_1. The ratios of the mass in $PM_{2.5}$ to that in PM_1 varied by OA factors. In this study, we further conducted the PMF analysis on combined inorganic and organic high-resolution mass spectra obtained by the LTOF-AMS to quantify organic nitrates (ONs) in PM_1 (see Sect. A in the SI for more details).

2.2 Offline analysis

During 21 December 2017 to 4 January 2018, $PM_{2.5}$ was collected on polytetrafluoroethylene (PTFE) filters (Whatman, pore size of 2 μm) by a four-channel sampler (Tianhong, TH-16A) at a flow rate of 16.7 L min^{-1}. Each sample corresponds to a 24-h period from 9:00 AM to 9:00 AM. The filters were stored in a freezer at -20°C before

analysis.[25] The filter samples were categorized into four groups representing different pollution levels on the basis of daily mean values of $PM_{2.5}$ concentrations and RH. The four categories were named as clean ($PM_{2.5}$ < 15 μg m^{-3}), dry haze ($PM_{2.5}$ > 35 μg m^{-3}, RH < 60%), humid haze ($PM_{2.5}$ > 35 μg m^{-3}, RH > 60%), and transition (15 μg m^{-3} < $PM_{2.5}$ < 35 μg m^{-3}) (Table S1 in the SI). The national primary ambient air quality standards for daily- and annual-mean $PM_{2.5}$ mass concentrations (i.e., 35 and 15 μg m^{-3}, respectively) were considered to separate clean and haze days. We chose 60% of RH to separate the humid and dry weather condition for haze days because that severe winter haze events in NCP were typically associated with high RH and that a previous study indicated particles having similar chemical compositions were plausibly in the liquid phase at RH > 60%.[1, 12] As listed in Table S1, the ALWC for dry-haze and humid-haze days were several and one hundred μg m^{-3}, respectively. Among these filters, two "humid haze" (YY/MM/DD, 17/12/28 and 17/12/29), two "clean" (17/12/22, 18/01/03), one "dry haze" (17/12/21), and one "transition" (18/01/04) samples were analysed by the Aerodyne I^--TOF-CIMS with the FIGAERO.[26] The transition period represented mixed clean and dry-haze conditions and the mass spectra showed intermediate features. The selection of the samples is explained in Sect. B of the SI.

In the FIGAERO offline analysis, a small area of the sample filters (0.196 cm^2) was punched off and placed between two clean Zefluor PTFE filters (Pall, pore size of 2 μm) in the FIGAERO. Samples were heated up from room temperature to 180°C in 20 minutes and stayed at 180°C for 10 minutes. Organic compounds were evaporated, carried by the carrier gas of ultra-high-purity nitrogen (UHP, >99.999%), ionized in the ion-molecule reaction (IMR) chamber, and sampled by the I^--TOF-CIMS. Three parallel samples were analysed for each filter. Background signals were obtained by analysing the blank PTFE filters with the same procedure as the ambient samples. For I^--TOF-CIMS, the average temperature (± 1 σ) of the ion-molecule reaction chamber was 45.7 ± 2.6°C and the pressure was 193 ± 21 mbar.

The mass spectra were acquired at a time resolution of one second and were analysed by Tofware (Tofwerk, version 2.5.10). The mass resolution of the instrument was 5000 to 6000 for ions of m/z > 200 Th. High-resolution peak fitting was performed for ions of m/z < 500 Th to ensure sufficient identification of ion formulae. Four ions, I^- (126.905 Th), $I(HNO_3)^-$ (189.901 Th), $I(CF_3COOH)^-$ (240.898), and I_3^- (380.714) were selected for mass calibration, and the mass accuracy was less than 10 ppm for individual ions throughout the experiment (Figure S2 in the SI). In total, 1881 ions clustered with I^- were identified (Figure S3 in the SI). These I^--adduct ions ($C_xH_yO_zX_n$, where X = S or N, x, y, $z \geq 1$ and n ≤ 2) contributed 90-97% of the total signals of the detected organic ions, which consists of 989 $C_xH_yO_z$, 856 $C_xH_yO_zN_n$, and 36 $C_xH_yO_zS_n$ I^--adduct ions. In the $C_xH_yO_zN_n$ category, 583 compounds with the formula of $C_xH_yO_zN_1$ (y is an odd number ≤ $2x$+3 and z≥4 except $C_6H_5NO_4$, $C_7H_7NO_4$, and $C_8H_9NO_4$ that were more likely nitrated phenols in urban environments) were tentatively designated as ONs.[27-30] Signal contributions of ions with two nitrogen or sulfur atoms are relatively minor. We also fitted three deprotonated organosulfate ions (i.e., $C_3H_5SO_5^-$, $C_2H_3SO_6^-$, $C_3H_5SO_6^-$) in the analysis. The 30-min temperature-dependent ion signals (i.e., so-called thermogram) during the temperature ramping and soaking stages were smoothed by the boxcar method and then integrated to yield the total signal intensity of each ion. The background signal intensity was then subtracted from the total signal intensity. The background-corrected signal intensity of each ion was normalized to the signal intensity of the reagent ion I^- to

represent the relative concentration of a specific molecule (normalized counts per second times second, ncps s). Most of the major ions showed unimodal thermograms (Figure S4 in the SI). The peak temperature where the highest signal appeared (T_{max}) was obtained.[26, 31]

Calibration experiments were conducted for a series of chemical compounds (Table S2 in the SI). Formic acid standard was produced by purging a commercial permeation tube (VICI, 23 ng min^{-1} at 50°C) with ultra-high-purity nitrogen. The liquid standards were deposited onto the filters in FIGAERO by using micro-syringes for calibration, including organic nitrates that were synthesized in the laboratory with purities of 54-72% and were diluted in hexane (Fisher Chemical, 95%)[20] and other compounds (Sigma-Aldrich, 98%) that were diluted in methanol (Fisher Chemical, 99.93%). Nitrophenols ($C_6H_5NO_3$ and $C_7H_7NO_3$) showed the highest sensitivities, followed by C_3-C_5 dicarboxylic acids ($C_4H_6O_4$ and $C_5H_8O_4$), oxalic acid ($C_2H_2O_4$), levoglucosan ($C_6H_{10}O_5$), phthalic acid ($C_8H_6O_4$), formic acid (CH_2O_2), and three hydroxyl ONs ($C_8H_9NO_4$, $C_7H_{15}NO_4$, and $C_8H_{17}NO_4$). We were unable to detect phenylethyl and heptyl nitrates ($C_8H_9NO_3$ and $C_7H_{15}NO_3$). The detected $C_6H_5NO_3$, $C_7H_7NO_3$, and $C_8H_9NO_3$ were plausibly nitrated phenols with one nitro group ($-NO_2$) and one hydroxyl group (-OH). The sensitivity of oxalic acid was lower than other dicarboxylic acids, similar to a previous study.[32] Our sensitivity of oxalic acid was two orders of magnitude greater than that reported by Lee et al. (2014). [32] We suspect that fast evaporation loss during deposition may happen in their study for volatile species like oxalic acid to cause an underestimation of the sensitivity. Moreover, the greater IMR pressure (i.e., 200 mbar) that was used in this study than in their study (i.e., 100 mbar) as well as other instrument-tuning differences may lead to sensitivity differences.[29] In general, we applied the average sensitivity (164.4 cps ppt^{-1}) of 4-nitrophenol and 2-methyl-4-nitrophenol for uncalibrated nitrated phenols and the average sensitivity (76.2 cps ppt^{-1}) of succinic acid and glutaric acid for $C_3H_4O_4$. The average sensitivity (8.7 cps ppt^{-1}) of the three hydroxyl ONs were applied for ONs. The average sensitivity (42.9 cps ppt^{-1}) of all calibrated compounds excluding nitrogen-containing ones were applied for other uncalibrated I^--adduct compounds. All sensitivities reported here were normalized to a million total reagent ion ($10^6 \times [I^-]$). Overall, the filter-based total mass concentrations of $C_xH_yO_zX_n \cdot I^-$ accounted for about 32-60% of SOA measured by the TOF-ACSM.

3 Results and discussion

3.1 Chemical composition of $PM_{2.5}$ and sources of OA

Figure 1 shows the time series of the mass concentrations of gas- and particle-phase pollutants measured in this study. The campaign-average (± one standard deviation) mass concentration of NR-$PM_{2.5}$ was 26.1 ± 33.9 μg m^{-3}, which was lower than the mean concentrations of 58.7 to 94.0 μg m^{-3} reported for previous winter campaigns in Beijing from 2008 to 2016.[3] The lower concentrations were perhaps due to meteorological conditions that facilitated dilution and transport of pollutants and effective emission control.[33, 34] Similar to the previous measurements,[3] OA accounted for the largest mass fraction (55%) of NR-$PM_{2.5}$ on average, followed by nitrate (19%), sulfate (12%), ammonium (11%), and chloride (3%). The campaign-average mass ratio of nitrate to sulfate was 1.6, which was higher than 0.6 to 1.4 reported previously for winter Beijing.[3] An even greater ratio of 2.1 was observed in winter in 2018 in Beijing.[35] The

increasing nitrate-to-sulfate ratio was consistent with significant reduction of sulfate but less efficient reduction of nitrate in the NCP.[36]

The PMF analysis identified six OA factors for $PM_{2.5}$, including four factors related to primary OA (POA) and two OOA factors. The former included hydrocarbon-like OA (HOA), cooking-related OA (COA), OA related to biomass burning (BBOA), and OA related to coal burning (CCOA). The OOA factors included more-oxygenated OOA (MO-OOA) and less-oxygenated OOA (LO-OOA). Figure S5 in the SI shows the mass spectra and the concentrations of the six factors. The overall characteristics of these OA factors for $PM_{2.5}$ were similar to those for PM_1 that were described by Zheng et al.[23] Briefly, the HOA factor showed predominant contributions from alkyl fragments (e.g., *m*/*z* 55, 57, 69, 71, and 83) and a good correlation with NO in concentration (Pearson's $R = 0.8$). The COA factor was distinguished by the high f_{55}/f_{57} ratio, and its concentration correlated with the signal intensities of a marker ion ($C_6H_{10}O^+$) obtained by the AMS for PM_1.[37] The CCOA factor was characterized by distinctive fragments (e.g., *m*/*z* 115, 128, 152, 165, 178, and 189) from polycyclic aromatic hydrocarbons (PAH). Moreover, the mass concentrations of CCOA were much lower than in previous studies,[3] for which recently introduced emission control on residential coal burning in northern China perhaps played a role. The relative intensities of *m*/*z* 60 and 73 were not distinct in the BBOA spectra because of prolonged thermal decomposition in the CV,[23] but the concentrations of BBOA correlated well with the signal intensities of the biomass-burning tracer ion of $C_2H_4O_2^+$ (i.e., for levoglucosan) measured by the concurrent AMS ($R = 0.6$) and the concentrations of gaseous acetonitrile (i.e., another biomass-burning tracer).

The CV-based mass spectra of the two OOA factors for $PM_{2.5}$ were dominated by *m*/*z* 44. Their concentrations showed different temporal variations. Specifically, the concentrations of LO-OOA correlated with acetaldehyde concentrations ($R = 0.68$) and showed a steady increase during daytime (Figure S6 in the SI), which might indicate photochemical production.[3, 7] The MO-OOA spectrum was distinguished by relatively greater signal intensities of *m*/*z* 29, 30, 31, and 58 compared to that of LO-OOA (Figure S5 in the SI), and showed better correlations ($R > 0.85$) with the signals of ions like $CH_{1\text{-}3}O^+$, $CH_3O_2^+$, $C_2O_2^+$, $C_2H_2O_2^+$, CHS^+, $CH_{2\text{-}4}SO_{1\text{-}3}^+$, CHN^+, $C_2H_7N^+$, and $C_3H_9N^+$ measured by the concurrent AMS (Figure S7 in the SI). The concentrations of MO-OOA correlated well with sulfate concentrations ($R = 0.98$) and RH ($R = 0.86$) and showed an afternoon valley in the mean diurnal profile (Figures S5 and S6). Previous studies hypothesized that aqueous processing was involved in the formation of this type of OOA for two reasons. First, the elevated sulfate concentrations during the severe haze event plausibly resulted from heterogeneous reactions on aqueous aerosols.[38] Second, the enhanced signals of $CH_{1\text{-}3}O^+$, $C_2H_2O_2^+$, and $CH_{2\text{-}4}SO_{1\text{-}3}^+$ during the severe haze event were perhaps from aqueous-processing products such as methanesulfonic acid (MSA) and glyoxal SOA.[39] The AMS fragments are however not unique tracers. For example, SOA produced by isoprene photooxidation also show high relative intensities of $CH_{1\text{-}3}O^+$ because of the contributions of hydroperoxides.[40] Therefore, more molecular information is needed to investigate the contribution of aqueous-processing to MO-OOA. On average, the total mass of the four primary factors contributed to about 41% of the OA mass, and the two OOA factors contributed to the rest of 59% in this study.

Haze days in NCP in winter are generally associated with stagnant conditions with low WS (e.g., < 1.5 m s^{-1} herein), while clean days are dominated by northern wind with high WS.[1] In our study, the worst pollution occurred on 17/12/27-17/12/29, showing the maximum NR-$PM_{2.5}$ mass loading of 191.0 μg m^{-3} and the highest RH of 90% (Figure 1). During the humid-haze days, the concentrations of NO_x and CO significantly increased while the changes of the SO_2 concentrations were insignificant. The concentrations of sulfate, nitrate, ammonium, and MO-OOA increased from several μg m^{-3} to up to 40 μg m^{-3} rapidly. As a result, the chemical composition of NR-$PM_{2.5}$ was different for the humid-haze, dry-haze, and clean cases (Table S1). OA contributed to over 65% of the $PM_{2.5}$ mass for the dry-haze and clean cases and about 40% of the $PM_{2.5}$ mass for the humid-haze case. SOA accounted for 50% during the dry-haze days and about 70% during the humid-haze days, suggesting enhanced secondary formation during humid-haze days. LO-OOA contributed most to the OOA mass during the dry-haze days, whereas the MO-OOA mass was greatly elevated and showed greater concentrations than LO-OOA during the humid-haze days. Greater ratios of MO-OOA/LO-OOA during the severe haze event (so-called "humid haze" herein) were similar to the findings of previous studies in Beijing.[3, 7] The mass loadings of POA and LO-OOA were 10-20% greater in $PM_{2.5}$ than in PM_1, whereas the mass loadings of MO-OOA were 1-1.3 times greater during the humid-haze days. The species $PM_{2.5}$-to-PM_1 mass ratio can be affected by hygroscopic growth, partitioning or dissolution, and condensed-phase reactions as well as changes of morphology that influences the viscosity and phase separation etc.[5, 41]

3.2 Molecular composition of SOA

The mean OA mass concentrations corresponding to the selected humid-haze, dry-haze, and clean-day filter samples were 46.1, 19.9, and 4.5 μg m^{-3}, respectively (Table 1). Figure S8 in the SI shows the average mass spectra of OA measured by the FIGAERO I^--TOF-CIMS. The detected ions were categorized into various groups on the basis of their molecular formulae. The total signal intensities of $C_xH_yO_zX_n \cdot I^-$ of the filter samples correlated well with the daily-mean OOA mass concentrations (R = 0.96) (Figure S9 in the SI). The signal intensities of individual ions in humid-haze samples were about 1-10 times greater than in dry-haze samples while the OOA mass loadings were 2-4 times greater (Figure S10 in the SI). Some oxygenated organic compounds cannot be detected efficiently by I^--TOF-CIMS, e.g., monoketones, monoaldehydes, monoalcohols, non-hydroxyl ONs, and some highly-oxygenated organic compounds. [32, 42] Mono-ketones, -aldehydes, and –alcohols are expected to be a minor portion of SOA in urban environment.[43] A previous study which measured the monocarbonyls in $PM_{2.5}$ in Xi'an, China showed a very low concentration of monocarbonyls (less than 20 ng m^{-3}).[44] The contributions of non-hydroxyl ONs and highly-oxygenated compounds with oxygen numbers greater than 6 were also expected to be small,[13, 20] although significant uncertainties remain the particle-phase quantification of them. To support, the average atomic oxygen-to-carbon ratios (O:C) ratios of the molecular composition (i.e., 0.65) agreed with the AMS results (i.e., 0.5 for LO-OOA and 0.78 for MO-OOA).

Figure 2 shows the relative ion signals grouped by their molecular formulae as well as their carbon and oxygen numbers. A study that was conducted in winter in 2018 in Beijing showed similar molecule compositions except that the relative signal intensities of sulfur-containing ions were smaller in our study (Figure S11 in the SI).[35] $C_xH_yO_z \cdot I^-$ ions were the most abundant for all cases, contributing to 60-70% of the total signal intensities in haze-day samples

and about 84% in clean-day samples (Figure 2a,b,c). Over 80% of the $C_xH_yO_z{\cdot}I^-$ signal intensities were contributed by compounds with carbon numbers of less than 10 (Figure 2d,e,f). In terms of oxygen number, major compounds contained 3-5 oxygen atoms. This was consistent with the volatility distribution of semi-volatile OOA.[45] Xu et al. found that 63% of OA were semi-volatile in summer in Beijing.[46] On the other hand, highly oxygenated organic molecules with 6 or more oxygen atoms might not be effectively detected in I^--TOF-CIMS because of their low sensitivities.[42] These compounds are important but perhaps a minor contributor to the OOA mass because of the formation of more-volatile products through the termination of RO_2 by NO_x in polluted urban environment.[47, 48]

$C_6H_yO_5$ compounds (mainly $C_6H_{10}O_5$) contributed largely to the signal intensities of $C_xH_yO_z{\cdot}I^-$ (Figure 2d,e,f). Levoglucosan can be a main contributor to the $C_6H_{10}O_5{\cdot}I^-$ signal in ambient environments.[49] Biomass burning and residential coal burning are the common sources of levoglucosan in winter in the NCP.[50] Residential coal burning has been largely reduced in the area in 2017.[23] The haze-day mass concentrations of BBOA were 5-7 times greater than those for clean days. Consistently, the haze-day signal intensities of $C_6H_{10}O_5{\cdot}I^-$ were 3-4 times greater than the clean-day intensities (Figure S10). Stagnant meteorological conditions lead to the accumulation of pollutants in haze days. The estimated mass concentrations of levoglucosan ranged from 83 to 612 ng m^{-3} in this study (Table 1), which was also consistent with the concentrations of 80-320 ng m^{-3} in $PM_{2.5}$ measured by other offline methods in winter in Beijing.[50] The BBOA concentrations were similar for dry and humid haze cases. The signal intensity of $C_6H_{10}O_5{\cdot}I^-$ was 30% greater in dry-haze samples than in humid-haze samples, for which the enhanced consumption of levoglucosan in aerosol water might explain.[51]

$C_xH_yO_4$ compounds showed the greatest signal enhancements during the humid-haze days. The relative signal contributions of $C_xH_yO_4$ compounds to the total ion intensities were 26.7%, 17.1%, and 14.5% for the humid-haze, dry-haze, and clean-day samples, respectively. Within the group of $C_xH_yO_4$, the signal intensities of short-chain compounds were much greater than the long-chain ones (Figure 2d,e,f). We defined the short-chain compounds as consisting of two series of species ($C_nH_{2n-2}O_4{\cdot}I^-$ where n = 2-6 and $C_nH_{2n-4}O_4{\cdot}I^-$ where n = 4-6), which were plausibly dicarboxylic acids. Low molecular weight dicarboxylic acids have been widely observed in ambient OA.[52] Previous offline measurements have shown that $C_3H_4O_4$, $C_4H_6O_4$, $C_5H_8O_4$, $C_6H_{10}O_4$, $C_4H_4O_4$, and $C_5H_6O_4$ in $PM_{2.5}$ were mainly malonic acid, succinic acid (or methylmalonic acid), glutaric acid (or methyl succinic acid), adipic acid (or methylglutaric acid), maleic acid (or fumaric acid), and methylmaleic acid, respectively, with daily-mean concentrations ranging from several to 207 ng m^{-3} in winter in Beijing.[53, 54] Consistently, the estimated total mass concentrations of these compounds herein ranged from 0.4 to 5.4, 7.2 to 26.6, and 37.3 to 131.5 ng m^{-3} for clean-day, dry-haze, and humid-haze samples, respectively.

Oxalic acid is the most abundant dicarboxylic acid in urban environments.[52] In this study, if the $C_2H_2O_4{\cdot}I^-$ represented oxalic acid, the estimated mass concentrations were 2-84 ng m^{-3}, which were much lower than previous offline findings of 45-1016 ng m^{-3}, especially for the haze days.[53] One explanation is that the detected $C_2H_2O_4{\cdot}I^-$ ions are likely from oxalate.[52] As shown in Table S3 in the SI, the first- and second-class dissolution constants (pK_{a1} = 1.25 and pK_{a2} =3.81) of oxalic acid are lower than the pH values of aerosols (i.e., 4-5) in northern China,[55] which allows the formation of

ammonium oxalate or oxalate metal complexes.[56] The thermal desorption in FIGAERO (i.e., < 180 °C) may not be suitable for detecting those compounds on the filters. The T_{max} value provides additional evidence for interpreting $C_2H_2O_4 \cdot I^-$. The T_{max} for $C_2H_2O_4 \cdot I^-$ in ambient samples was 143.2°C, which is much higher than the T_{max} value for pure oxalic acid (38.3°C). T_{max} may be affected by the concentration and surface area of the calibrant solutions after depositing on the filter in FIGAERO.[57] We found that T_{max} largely depended on the existing form of the compound. Indeed, the T_{max} of ammonium oxalate was 69.1°C in methanol but over 100°C when oversaturated in water (Figure S12 in the SI). On the other hand, the T_{max} values generally increased as the molecular weight increases, ranging from 60 to 120 °C. For $C_2H_2O_4$ and $C_3H_4O_4$, the T_{max} values were however significant greater than other O_4 compounds (Figure S13 in the SI). Based on their thermograms, we cannot exclude the possibility of these small ions being thermal fragmentation products (Figure S4 and Table S3 in the SI). By contrast, the T_{max} values of $C_4H_6O_4$, $C_5H_8O_4$, and $C_6H_{10}O_4$ for the ambient samples were close to the values of pure succinic acid, glutaric acid, and adipic acid. These compounds have greater pK_{a1} and pK_{a2} values of 4 to 6 (Table S3) and thus are more difficult to form salts than oxalic acid. Laboratory studies have shown that the neutralization with ammonia dramatically reduces the volatility of oxalic acid but has no significant impact on adipic acid ($C_6H_{10}O_4$).[58]

Figure 3 shows the comparison of the signal intensities of $C_xH_yO_z \cdot I^-$ ions for humid-haze days with those for dry-haze days. The concentration ratios of the $C_nH_{2n-2}O_4$ (n = 2-6) and $C_nH_{2n-4}O_4$ (n = 4-6) compounds to POA were 3-19 times greater in humid-haze than in dry-haze samples, suggesting enhanced secondary formation of dicarboxylic acids during the severe haze event. These compounds were plausibly part of the MO-OOA. The MO-OOA-to-POA ratios were 3-6 times larger during the humid-haze days than during the dry-haze days (Figure 1e). The enhanced formation of dicarboxylic acids may explain the high O:C ratios (i.e., 0.78) of MO-OOA in PM_1.[23] Both primary and secondary sources may contribute to dicarboxylic acids in winter in Beijing.[53] The elevated ALWC promoted the dissolution of these water-soluble gases into aerosol water to increase the SOA mass.[13] The oxidation of soluble organic precursors (e.g., glyoxal, methyl glyoxal, pyruvic acid, etc.) in aqueous aerosols is an important pathway to produce dicarboxylic acids and to promote the uptake of carbonyls and acids.[52, 59, 60] A recent study has shown five to six orders of magnitude greater gas-to-particle partitioning coefficients for glyoxal and formaldehyde than the theoretically predicted values in winter in Beijing, suggesting potentially important contributions of condensed phase reactions to these diacids.[61] Moreover, high concentrations of ammonia in the NCP may escalate the SOA yield from the aqueous processing of glyoxal.[62] Photochemical degradation of condensed phase long-chain diacids may happen to produce short-chain ones.[63]

Other ion series showed > 3 times enhanced signal (normalized to the POA loadings) during humid-haze compared to dry-haze samples, and may therefore be associated with MO-OOA as well. For example, $C_8H_6O_4$ and $C_nH_{2n}O_4$ (n = 3-6) were enriched in the humid-haze samples. Although there are many structure possibilities, their formulae are consistent with common atmospheric oxidation products. $C_8H_6O_4$ was likely phthalic acid that could be produced by aromatic oxidation (e.g., the photooxidation of naphthalene).[64] $C_4H_8O_4$ might be 2-methylglyceric acid that could be produced in the condensed phase by further reactions of isoprene oxidation products under high NO_x conditions.[65] Acids are water-soluble, and therefore the promoted dissolution to aqueous aerosols may explain the elevated particle-

phase concentrations of acids. $C_6H_8O_4$ could be the methylglyoxal dimer, while $C_6H_{10}O_4$ and $C_6H_{12}O_4$ have been observed as the products of methylglyoxal in aqueous aerosol mimics although the formation mechanism remains unclear.[66, 67] For $O_{\geq 5}$ compounds, $C_6H_{4,6}O_5$, $C_7H_{6,8}O_5$, and $C_9H_6O_5$ were enriched in the humid-haze samples. The former two were typical close-shell products that might be formed by the photooxidation of light aromatic compounds via the bicyclic peroxy radical pathway.[48] Additionally, highly oxygenated compounds with low degree of unsaturation such as $C_nH_{2n-2}O_8$ (n = 11, 12, 14, 15) with double bond equivalents (DBE) of 2 and $C_nH_{2n-4}O_9$ (n = 10, 13, DBE = 3) were enriched in the humid-haze samples. The values of DBE were calculated following the equation DBE = 1 + nC – nH/2 + nN/2, where nC, nH, and nN refer to the number of carbon, hydrogen, and nitrogen atoms in the formulae. A recent study indicated that long-chain cyclic alkanes could undergo autoxidation efficiently under ambient conditions even with high concentrations of NO_x to produce similar O_8 and O_9 molecules.[68] The potential role of the autoxidation of long-chain alkanes in the SOA formation in polluted urban environment has not yet been well studied. Another explanation of the $C_nH_{2n-2}O_8$ and $C_nH_{2n-4}O_9$ compounds is oligomerization for which the formation of oligomeric products may be favoured in aqueous aerosols.[69]

Nitrogen-containing ions ($C_xH_yO_zN_{1-2}\cdot I^-$) accounted for 15-35% of the total ion intensities and their relative signal contributions were much greater in haze-day samples than in clean-day samples (Figure 2a,b,c). These compounds might be nitrated phenols (-NO_2), ONs such as non-peroxy (-ONO_2), peroxy (-$OONO_2$), and peroxyacyl (-(O)$OONO_2$) nitrates, or nitrogen-containing products from the carbonyl and ammonia (or amine) reactions (e.g., -CON-).[20, 27, 67, 69, 70] $C_{5\text{-}7}H_yO_{3\text{-}4}N_{1\text{-}2}\cdot I^-$ was the major group of detected nitrogen-containing ions (Figure 2g,h,i), which was similar to the findings of the later study in 2018 in Beijing.[35] In this group, major ions such as $C_6H_5NO_3$, $C_7H_7NO_3$, $C_6H_5NO_4$, and $C_7H_7NO_4$ were likely to be contributed predominantly by nitrated phenols. The total particle-phase concentrations of these compounds were 3 to 156 ng m^{-3}, which agreed with the reported concentration range of corresponding nitrated phenols (several to 300 ng m^{-3}) in the NCP in winter.[71-73] The signal intensities of these molecules in haze-day samples were 1-2 orders of magnitude larger than in clean-day samples (Figure S10 in the SI). In particular, the signal enhancement compared to clean days was the greatest for $C_6H_5NO_3$ that was assigned tentatively as nitrophenol. Coal burning, biomass burning, and vehicle exhaust are typical primary sources of nitrated phenols in urban areas.[71] Online measurements of gaseous nitrated phenols indicated strong photochemical secondary formation of these species in Beijing.[28] Both primary and secondary sources may be enhanced under haze conditions because of the stagnant meteorological conditions and high precursor concentrations. The relative enhancements of these nitrated phenols to POA for the humid-haze days were 2-3 times greater than that for the dry-haze days, to which aqueous production of nitrated phenols might also contribute to the enhancement.[74]

ONs are important secondary products formed from the OH- or NO_3-initiated oxidation of gaseous organic compounds in the presence of NO_x in urban environments.[75, 76] The average formulae of particle-phase ONs for the humid-haze, dry-haze, and clean-day samples were $C_{8.9}H_{14.6}O_{6.0}N_{1.0}$, $C_{9.0}H_{15.1}O_{6.0}N_{1.0}$, and $C_{6.2}H_{9.4}O_{5.4}N_{1.0,}$ respectively. They were quite different from the average formula of ONs (i.e., $C_{11.4}H_{16.2}O_{8.1}N_{1.0}$) measured at a rural site in Germany in summer.[77] Biogenic VOCs (e.g., monoterpenes and sesquiterpenes) are important precursors in summer that may lead to ONs with high carbon numbers in the study in Germany. The average formula of ONs for clean days herein was

consistent with light aromatic compounds being as important precursors, whereas the low degree of unsaturation of ONs for haze days suggested that anthropogenic precursors such as alkanes or alkenes perhaps play an important role. ONs for the two haze cases accounted for a similar fraction of 15-16% of the total signal intensities (Figure 2). By contrast, the relative signal intensity of ONs for clean days was 3%. The mass concentrations of ONs in $PM_{2.5}$ estimated from the FIGAERO I^--TOF-CIMS measurements were 7.0, 2.4, and 0.03 μg m^{-3} for the humid-haze, dry-haze, and clean-day cases, respectively. The mass concentrations of ONs in PM_1 estimated by the PMF method from the AMS data were 3.4-7.9, 3.3-5.0, and 0.6-1.1 μg m^{-3}, respectively, which was similar to the semi-quantification of the FIGAERO I^--TOF-CIMS data (Section A in the SI). The campaign-average mass concentration of $NO_{3,org}$ (NO^+_{org}+$NO^+_{2,org}$) in PM_1 obtained from the AMS data in our study was 0.60 ± 0.58 μg m^{-3}, which were similar to the result of 0.7 μg m^{-3} from a previous study in the NCP in winter.[78] In addition, the signal intensities of the $C_xH_yN_{1-2}$ fragments in the AMS spectra were much lower than those of the ON fragments, suggesting a minor contribution of nitrogen-containing products from the carbonyl and ammonia (or amine) reactions.[79] Non-oxygenated amines and imidazole containing compounds cannot be detected efficiently by I^--TOF-CIMS.

Figure 4 shows the mass spectra of ONs for the humid- and dry-haze cases that are categorized by their carbon numbers. The signal intensities of ONs were mainly contributed by O_{4-7} compounds in all carbon groups (Figure 4a,b,c). By contrast, the major ON molecules were O_{6-8} compounds in rural or near-forest areas,[77, 80] which might be explained by the predominant biogenic contributions to ONs in the rural or near-forest areas in summer versus anthropogenic contributions in urban environments in winter. On the basis of the carbon number and the degree of saturation of ON formulae, we hypothesize that the main precursors of ONs in Beijing likely include aromatics, alkanes, and alkenes.[20, 48, 81] Comparing the two haze cases, the dry-haze sample has more abundant ONs with carbon numbers of 5 to 10, whereas the humid-haze samples have more $C_{<5}$ or $C_{>10}$ ON molecules (Figure 4 d,e,f). Hydrolysis of ONs may happen in aerosol water and possibly decrease the abundance of C_{5-10} ONs in humid-haze samples.[82] The short-chain ONs ($C_{<5}$) may be formed via non-radical reactions between dissolved aldehydes or alcohols with HNO_3 in wet aerosols.[83] The $C_{>10}$ ONs consisted of multiple molecules with low degree of unsaturation (DBE = 2,3), which was similar to the $C_nH_{2n-2}O_8$ (n = 11, 12, 14, 15, DBE = 2) and $C_nH_{2n-4}O_9$ (n = 10, 13, DBE = 3) compounds discussed before. The mechanism that leads to the enhanced signals of those long-chain ONs during the severe haze event remains unknown.

Additionally, organosulfates are important aqueous-reaction products.[84] The I^--TOF-CIMS identified some organosulfate compounds.[85, 86] As shown in Figure 2a,b,c, the signal intensities of detected $C_xH_yO_zS_m \cdot I^-$ ions were greatly elevated in humid-haze samples, which mighy contribute to the MO-OOA mass. $CH_4SO_3 \cdot I^-$ had the greatest signal intensity among the $C_xH_yO_zS_m \cdot I^-$ ions and was likely MSA. The concentrations of CH_4SO_3 in humid-haze samples were over 20 times larger than in dry-haze samples. MSA is mainly formed by the aqueous uptake and oxidation of dimethyl sulfide or dimethyl sulfoxide[87, 88] and thus its formation may be enhanced under humid-haze conditions. Emissions of terrestrial sources (e.g., waste disposals) are the main sources of dimethyl sulfide and dimethyl sulfoxide in Beijing.[89] The MSA concentration can roughly be estimated with empirical parameterizations on the basis of the fragment signals of $CH_3SO_2^+$ measured by AMS.[90] Our AMS data suggested average concentrations of 0.02 μg m^{-3} of MSA for clean days and 0.6 μg m^{-3} for humid-haze days, which were within the same order of

magnitude of previous findings in Beijing.[89] The signal intensities of $CH_4SO_3 \cdot I^-$ also showed a good correlation with the AMS-derived MSA concentrations (R = 0.96) (Figure S14 in the SI). Moreover, three types of organosulfates ($C_3H_5SO_5^-$, $C_2H_3SO_6^-$, and $C_3H_5SO_6^-$) were identified and may be part of MO-OOA. Their signal intensities were elevated greatly in humid-haze days (Figure S15 in the SI). These organosulfates have been assigned as hydroxyacetone sulfate ($C_3H_5SO_5^-$), glycolic acid sulfate ($C_2H_3SO_6^-$), and lactic acid sulfate ($C_3H_5SO_6^-$) in other studies.[85, 86] Glycolic acid sulfate was the most abundant organosulfate in Beijing, which might be formed by the uptake of glyoxal in liquid ammonium sulfate aerosols.[85, 86, 91].

3.3 Precursors and pathways leading to enhanced SOA formation during the severe haze event

Figure 5a shows the relative contribution of OOAs to the elevated SOA mass in $PM_{2.5}$ during the severe haze event (humid-haze) in comparison with the less polluted case (dry-haze) and the corresponding molecular composition, both normalized by the POA mass concentrations. On average, 88% of the SOA enhancement during the severe haze event was attributed to MO-OOA and 12% of the enhancement was from LO-OOA. The mass spectra of MO-OOA showed much higher relative signal intensities from $CH_{1\text{-}3}O^+$, $CH_3O_2^+$, $C_2H_2O_2^+$, and CO_2^+ (Figure 5b), leading to a greater O:C ratio of MO-OOA than that of LO-OOA.[92] The molecular composition analysis showed that $C_{6\text{-}9}$-ONs, $C_{\geq 10}$-ONs, and $C_xH_yO_4$ compounds were the major components corresponding to the enhanced SOA (i.e., 65% in total) or MO-OOA mass. The large contribution of $C_{6\text{-}9}$- and $C_{\geq 10}$-ONs highlights the potential importance of aromatic and long-chain alkane/alkene as SOA precursors in winter in polluted urban environments. The $C_xH_yO_4$ compounds included dicarboxylic acids and the oxidation products that were likely from isoprene and aromatics as well as the oligomers or products from methylglyoxal aqueous uptake. During the severe haze event, the ALWC reached 100 ± 83 μg m^{-3}. The enrichment of the $C_{6\text{-}9}$-ONs, $C_{\geq 10}$-ONs, and $C_xH_yO_4$ compounds in the particle phase was plausibly associated with the elevated ALWC. However, the relative contribution of promoted dissolution or aqueous-phase production to the enrichment of these ONs and O_4 compounds remains unclear. Oligomerization can be significantly enhanced in wet aerosols.[67, 69] Promoted dissolution might be caused by the enhanced formation in the gas phase, in which elevated NO_x concentrations likely played a role especially for ONs. Additionally, nitrated phenols, organosulfates, and MSA were important part of MO-OOA, although their relative contributions to the elevated SOA mass during the severe haze event were small (< 2%).

The results indicate that various precursors and processes can be involved in the SOA formation in polluted urban environments. Nitrogen-containing species, in particular ONs, contribute the most to the enhanced SOA formation during the severe haze event. The I^--TOF-CIMS is not sensitive to phenylethyl and heptyl nitrates in our calibration experiments, and therefore the observed ONs, in agreement with the AMS-derived ONs in mass, are plausibly multifunctional (e.g., with a hydroxyl group). The dissolution of these compounds to aerosol water may be promoted by the elevated ALWC to lead to the enrichment during the severe haze event. On the other hand, the gas-phase production of ONs may be enhanced by elevated NO_x levels under haze conditions. The reduction of NO_x is therefore important for future SOA control in China. The reduction of nitrate is also important because it affects the ALWC and thus the promotion of aqueous SOA formation when high RH presents in winter in NCP. Additionally, highly

oxygenated long-chain molecules ($C_xH_yO_z$ and $C_xH_yO_zN$, $15 \geq x \geq 10$) that may or may not contain nitrogen atoms are enriched in the humid-haze samples. These compounds may be oligomers or the autooxidation products of long-chain alkanes or alkenes, which calls further research to understand their formation mechanism as well as the humidity impacts on their formation.

Supporting Information

The supporting information is available free of charge on the ACS Publications website.

Descriptions and diagnostics of the PMF solution selection, quantification of organic nitrates, calibrated sensitivities of the selected compounds, high-resolution peak fitting and thermograms of major ions, mass spectra and time-series of the PMF factors, the molecular compositions under different haze conditions, distribution of the mean T_{max}, and comparisons of the mass spectra of the parallel samples.

Notes

The authors declare no competing financial interest.

Acknowledgments

This work was supported by the National Natural Science Foundation of China (41875165, 41961134034, 51861135102), the MOST National Key R&D Program of China (2017YFC0213000, Task 3), the 111 Project of Urban Air Pollution and Health Effects (B20009), and the European Research Council with the grant CHAPAs (Nr. 850614). Manish Shrivastava was supported by the U.S. DOE, Office of Science, Office of Biological and Environmental Research, through the Early Career Research Program. The Pacific Northwest National Laboratory is operated for DOE by the Battelle Memorial Institute under contract DE-AC06-76RL01830. The authors gratefully acknowledge Yele Sun, Jordan Krechmer, Philip Croteau, and Manjula Canagaratna for technical support and helpful discussion.

References

1. An, Z. S.; Huang, R. J.; Zhang, R. Y.; Tie, X. X.; Li, G. H.; Cao, J. J.; Zhou, W. J.; Shi, Z. G.; Han, Y. M.; Gu, Z. L.; Ji, Y. M., Severe haze in northern China: A synergy of anthropogenic emissions and atmospheric processes. *Proc. Natl. Acad. Sci. U. S. A.* **2019,** *116*, (18), 8657-8666.
2. Huang, R. J.; Zhang, Y. L.; Bozzetti, C.; Ho, K. F.; Cao, J. J.; Han, Y. M.; Daellenbach, K. R.; Slowik, J. G.; Platt, S. M.; Canonaco, F.; Zotter, P.; Wolf, R.; Pieber, S. M.; Bruns, E. A.; Crippa, M.; Ciarelli, G.; Piazzalunga, A.; Schwikowski, M.; Abbaszade, G.; Schnelle-Kreis, J.; Zimmermann, R.; An, Z. S.; Szidat, S.; Baltensperger, U.; El Haddad, I.; Prevot, A. S. H., High secondary aerosol contribution to particulate pollution during haze events in China. *Nature* **2014,** *514*, (7521), 218-222.
3. Duan, J.; Huang, R. J.; Li, Y.; Chen, Q.; Zheng, Y.; Chen, Y.; Lin, C.; Ni, H.; Wang, M.; Ovadnevaite, J.; Ceburnis, D.; Chen, C.; Worsnop, D. R.; Hoffmann, T.; O'Dowd, C.; Cao, J., Summertime and wintertime atmospheric processes of secondary aerosol in Beijing. *Atmos. Chem. Phys.* **2020,** *20*, (6), 3793-3807.
4. Huang, R. J.; Wang, Y. C.; Cao, J. J.; Lin, C. S.; Duan, J.; Chen, Q.; Li, Y. J.; Gu, Y. F.; Yan, J.; Xu, W.; Frohlich, R.; Canonaco, F.; Bozzetti, C.; Ovadnevaite, J.; Ceburnis, D.; Canagaratna, M. R.; Jayne, J.; Worsnop, D. R.; El-Haddad, I.; Prevot, A. S. H.; O'Dowd, C. D., Primary emissions versus secondary formation of fine particulate matter in the most polluted city (Shijiazhuang) in North China. *Atmos. Chem. Phys.* **2019,** *19*, (4), 2283-2298.
5. Sun, Y. L.; He, Y.; Kuang, Y.; Xu, W. Y.; Song, S. J.; Ma, N.; Tao, J. C.; Cheng, P.; Wu, C.; Su, H.; Cheng, Y. F.; Xie, C. H.; Chen, C.; Lei, L.; Qiu, Y. M.; Fu, P. Q.; Croteau, P.; Worsnop, D. R., Chemical Differences Between PM_1 and $PM_{2.5}$ in Highly Polluted Environment and Implications in Air Pollution Studies. *Geophys. Res. Lett.* **2020,** *47*, (5).
6. Lu, K. D.; Fuchs, H.; Hofzumahaus, A.; Tan, Z. F.; Wang, H. C.; Zhang, L.; Schmitt, S. H.; Rohrer, F.; Bohn, B.; Broch, S.; Dong, H. B.; Gkatzelis, G. I.; Hohaus, T.; Holland, F.; Li, X.; Liu, Y.; Liu, Y. H.; Ma, X. F.; Novelli, A.; Schlag, P.; Shao, M.; Wu, Y. S.; Wu, Z. J.; Zeng, L. M.; Hu, M.; Kiendler-Scharr, A.; Wahner, A.; Zhang, Y. H., Fast photochemistry in wintertime haze: consequences for pollution mitigation strategies. *Environ. Sci. Technol.* **2019,** *53*, (18), 10676-10684.
7. Xu, W. Q.; Han, T. T.; Du, W.; Wang, Q. Q.; Chen, C.; Zhao, J.; Zhang, Y. J.; Li, J.; Fu, P. Q.; Wang, Z. F.; Worsnop, D. R.; Sun, Y. L., Effects of aaqueous-phase and photochemical pprocessing on secondary organic aerosol formation and evolution in Beijing, China. *Environ. Sci. Technol.* **2017,** *51*, (2), 762-770.
8. Ulbrich, I. M.; Canagaratna, M. R.; Zhang, Q.; Worsnop, D. R.; Jimenez, J. L., Interpretation of organic components from Positive Matrix Factorization of aerosol mass spectrometric data. *Atmos. Chem. Phys.* **2009,** *9*, (9), 2891-2918.
9. Ng, N. L.; Canagaratna, M. R.; Zhang, Q.; Jimenez, J. L.; Tian, J.; Ulbrich, I. M.; Kroll, J. H.; Docherty, K. S.; Chhabra, P. S.; Bahreini, R., Organic aerosol components observed in Northern Hemispheric datasets from Aerosol Mass Spectrometry. *Atmos. Chem. Phys.* **2010,** *10*, (10), 4625-4641.
10. Zhang, Q.; Jimenez, J. L.; Canagaratna, M. R.; Ulbrich, I. M.; Ng, N. L.; Worsnop, D. R.; Sun, Y., Understanding atmospheric organic aerosols via factor analysis of aerosol mass spectrometry: a review. *Anal. Bioanal. Chem.* **2011,** *401*, (10), 3045-67.
11. Wang, J. F.; Ye, J. H.; Zhang, Q.; Zhao, J.; Wu, Y. Z.; Li, J. Y.; Liu, D. T.; Li, W. J.; Zhang, Y. G.; Wu, C.; Xie, C. H.; Qin, Y. M.; Lei, Y. L.; Huang, X. P.; Guo, J. P.; Liu, P. F.; Fu, P. Q.; Li, Y. J.; Lee, H. C.; Choi, H. W.; Zhang, J.; Liao, H.; Chen, M. D.; Sun, Y. L.; Ge, X. L.; Martin, S. T.; Jacob, D. J., Aqueous production of secondary organic aerosol from fossil-fuel emissions in winter Beijing haze. *Proc. Natl. Acad. Sci. U. S. A.* **2021,** *118*, (8), e2022179118.
12. Liu, Y. C.; Wu, Z. J.; Wang, Y.; Xiao, Y.; Gu, F. T.; Zheng, J.; Tan, T. Y.; Shang, D. J.; Wu, Y. S.; Zeng, L. M.; Hu, M.; Bateman, A. P.; Martin, S. T., Submicrometer particles are in the liquid state during heavy haze episodes in the urban atmosphere of Beijing, China. *Environ. Sci. Technol. Lett.* **2017,** *4*, (10), 427-432.
13. Gkatzelis, G. I.; Papanastasiou, D. K.; Karydis, V. A.; Hohaus, T.; Liu, Y.; Schmitt, S. H.; Schlag, P.; Fuchs, H.; Novelli, A.; Chen, Q.; Cheng, X.; Broch, S.; Dong, H.; Holland, F.; Li, X.; Liu, Y.; Ma, X.; Reimer, D.; Rohrer, F.; Shao, M.; Tan, Z.; Taraborrelli, D.; Tillmann, R.; Wang, H.; Wang, Y.; Wu, Y.; Wu, Z.; Zeng, L.; Zheng, J.; Hu, M.; Lu, K.; Hofzumahaus, A.; Zhang, Y.; Wahner, A.; Kiendler-Scharr, A., Uptake of water-soluble gas-phase oxidation products drives organic particulate pollution in Beijing. *Geophys. Res. Lett.* **2021,** *48*, (8), e2020GL091351.
14. Herrmann, H.; Schaefer, T.; Tilgner, A.; Styler, S. A.; Weller, C.; Teich, M.; Otto, T., Tropospheric aqueous-phase chemistry: kinetics, mechanisms, and its coupling to a changing gas phase. *Chem. Rev.* **2015,** *115*, (10), 4259-4334.
15. El-Sayed, M. M. H.; Wang, Y. Q.; Hennigan, C. J., Direct atmospheric evidence for the irreversible formation of aqueous secondary organic aerosol. *Geophys. Res. Lett.* **2015,** *42*, (13), 5577-5586.
16. Gilardoni, S.; Massoli, P.; Paglione, M.; Giulianelli, L.; Carbone, C.; Rinaldi, M.; Decesari, S.; Sandrini, S.; Costabile, F.; Gobbi, G. P.; Pietrogrande, M. C.; Visentin, M.; Scotto, F.; Fuzzi, S.; Facchini, M. C., Direct observation of aqueous secondary organic aerosol from biomass-burning emissions. *Proc. Natl. Acad. Sci. U. S. A.* **2016,** *113*, (36), 10013-10018.
17. Kuang, Y.; He, Y.; Xu, W.; Yuan, B.; Zhang, G.; Ma, Z.; Wu, C.; Wang, C.; Wang, S.; Zhang, S.; Tao, J.; Ma, N.; Su, H.; Cheng, Y.; Shao, M.; Sun, Y., Photochemical aqueous-phase reactions induce rapid daytime formation of oxygenated organic aerosol on the North China Plain. *Environ. Sci. Technol.* **2020,** 54, (7), 3849–3860.
18. Tong, Y.; Pospisilova, V.; Qi, L.; Duan, J.; Gu, Y.; Kumar, V.; Rai, P.; Stefenelli, G.; Wang, L.; Wang, Y.; Zhong, H.; Baltensperger, U.; Cao, J.; Huang, R. J.; Prévôt, A. S. H.; Slowik, J. G., Quantification of solid fuel combustion and aqueous chemistry contributions to secondary organic aerosol during wintertime haze events in Beijing. *Atmos. Chem. Phys.* **2021,** *21*, (12), 9859-9886.
19. Shrivastava, M.; Andreae, M. O.; Artaxo, P.; Barbosa, H. M. J.; Berg, L. K.; Brito, J.; Ching, J.; Easter, R. C.; Fan, J. W.; Fast, J. D.; Feng, Z.; Fuentes, J. D.; Glasius, M.; Goldstein, A. H.; Alves, E. G.; Gomes, H.; Gu, D.; Guenther, A.; Jathar, S. H.; Kim, S.; Liu, Y.; Lou, S. J.; Martin, S. T.; McNeill, V. F.; Medeiros, A.; de Sa, S. S.; Shilling, J. E.; Springston, S. R.; Souza, R.

A. F.; Thornton, J. A.; Isaacman-VanWertz, G.; Yee, L. D.; Ynoue, R.; Zaveri, R. A.; Zelenyuk, A.; Zhao, C., Urban pollution greatly enhances formation of natural aerosols over the Amazon rainforest. *Nat. Commun.* **2019,** *10*, 1046.
20. Shi, X. D.; Qiu, X. H.; Cheng, Z.; Chen, Q.; Rudich, Y.; Zhu, T., Isomeric identification of particle-phase organic nitrates through Gas Chromatography and Time-of-Flight Mass Spectrometry coupled with an Electron Capture Negative Ionization Source. *Environ. Sci. Technol.* **2020,** *54*, (2), 707-713.
21. Hu, W. W.; Hu, M.; Hu, W.; Jimenez, J. L.; Yuan, B.; Chen, W. T.; Wang, M.; Wu, Y. S.; Chen, C.; Wang, Z. B.; Peng, J. F.; Zeng, L. M.; Shao, M., Chemical composition, sources, and aging process of submicron aerosols in Beijing: Contrast between summer and winter. *J. Geophys. Res.-Atmos.* **2016,** *121*, (4), 1955-1977.
22. Canagaratna, M. R.; Jayne, J. T.; Jimenez, J. L.; Allan, J. D.; Alfarra, M. R.; Zhang, Q.; Onasch, T. B.; Drewnick, F.; Coe, H.; Middlebrook, A., Chemical and microphysical characterization of ambient aerosols with the aerodyne aerosol mass spectrometer. *Mass Spectrom. Rev.* **2007,** *26*, (2), 185-222.
23. Zheng, Y.; Cheng, X.; Liao, K.; Li, Y.; Li, Y. J.; Huang, R. J.; Hu, W.; Liu, Y.; Zhu, T.; Chen, S.; Zeng, L.; Worsnop, D. R.; Chen, Q., Characterization of anthropogenic organic aerosols by TOF-ACSM with the new capture vaporizer. *Atmos. Meas. Tech.* **2020,** *13*, (5), 2457-2472.
24. Paatero, P.; Tapper, U., Positive Matrix Factorization - A nonnegative factor model with optimal utilization of error-estimates of data values. *Environmetrics* **1994,** *5*, (2), 111-126.
25. Fang, Y. H.; Ye, C. X.; Wang, J. X.; Wu, Y. S.; Hu, M.; Lin, W. L.; Xu, F. F.; Zhu, T., Relative humidity and O-3 concentration as two prerequisites for sulfate formation. *Atmos. Chem. Phys.* **2019,** *19*, (19), 12295-12307.
26. Lopez-Hilfiker, F. D.; Mohr, C.; Ehn, M.; Rubach, F.; Kleist, E.; Wildt, J.; Mentel, T. F.; Lutz, A.; Hallquist, M.; Worsnop, D.; Thornton, J. A., A novel method for online analysis of gas and particle composition: description and evaluation of a Filter Inlet for Gases and AEROsols (FIGAERO). *Atmos. Meas. Tech.* **2014,** *7*, (4), 983-1001.
27. Huang, W.; Saathoff, H.; Shen, X. L.; Ramisetty, R.; Leisner, T.; Mohr, C., Seasonal characteristics of organic aerosol chemical composition and volatility in Stuttgart, Germany. *Atmos. Chem. Phys.* **2019,** *19*, (18), 11687-11700.
28. Cheng, X.; Chen, Q.; Li, Y. J.; Huang, G. C.; Liu, Y.; Lu, S. H.; Zheng, Y.; Qiu, W. Y.; Lu, K. D.; Qiu, X. H.; Bianchi, F.; Yan, C.; Yuan, B.; Shao, M.; Wang, Z.; Canagaratna, M. R.; Zhu, T.; Wu, Y. S.; Zeng, L. M., Secondary production of gaseous nitrated phenols in polluted urban environments. *Environ. Sci. Technol.* **2021,** *55*, (8), 4410–4419.
29. Ye, C.; Yuan, B.; Lin, Y.; Wang, Z.; Hu, W.; Li, T.; Chen, W.; Wu, C.; Wang, C.; Huang, S.; Qi, J.; Wang, B.; Wang, C.; Song, W.; Wang, X.; Zheng, E.; Krechmer, J. E.; Ye, P.; Zhang, Z.; Wang, X.; Worsnop, D. R.; Shao, M., Chemical characterization of oxygenated organic compounds in the gas phase and particle phase using iodide CIMS with FIGAERO in urban air. *Atmos. Chem. Phys.* **2021,** *21*, (11), 8455-8478.
30. Mehra, A.; Canagaratna, M.; Bannan, T. J.; Worrall, S. D.; Bacak, A.; Priestley, M.; Liu, D.; Zhao, J.; Xu, W.; Sun, Y.; Hamilton, J. F.; Squires, F. A.; Lee, J.; Bryant, D. J.; Hopkins, J. R.; Elzein, A.; Budisulistiorini, S. H.; Cheng, X.; Chen, Q.; Wang, Y.; Wang, L.; Stark, H.; Krechmer, J. E.; Brean, J.; Slater, E.; Whalley, L.; Heard, D.; Ouyang, B.; Acton, W. J. F.; Hewitt, C. N.; Wang, X.; Fu, P.; Jayne, J.; Worsnop, D.; Allan, J.; Percival, C.; Coe, H., Using highly time-resolved online mass spectrometry to examine biogenic and anthropogenic contributions to organic aerosol in Beijing. *Faraday Discuss.* **2021,** *226*, 382-408.
31. Bannan, T. J.; Le Breton, M.; Priestley, M.; Worrall, S. D.; Bacak, A.; Marsden, N. A.; Mehra, A.; Hammes, J.; Hallquist, M.; Alfarra, M. R.; Krieger, U. K.; Reid, J. P.; Jayne, J.; Robinson, W.; McFiggans, G.; Coe, H.; Percival, C. J.; Topping, D., A method for extracting calibrated volatility information from the FIGAERO-HR-ToF-CIMS and its experimental application. *Atmos. Meas. Tech.* **2019,** *12*, (3), 1429-1439.
32. Lee, B. H.; Lopez-Hilfiker, F. D.; Mohr, C.; Kurten, T.; Worsnop, D. R.; Thornton, J. A., An Iodide-Adduct High-Resolution Time-of-Flight Chemical-Ionization Mass Spectrometer: application to atmospheric inorganic and organic compounds. *Environ. Sci. Technol.* **2014,** *48*, (11), 6309-6317.
33. Zhang, Q.; Zheng, Y.; Tong, D.; Shao, M.; Wang, S.; Zhang, Y.; Xu, X.; Wang, J.; He, H.; Liu, W.; Ding, Y.; Lei, Y.; Li, J.; Wang, Z.; Zhang, X.; Wang, Y.; Cheng, J.; Liu, Y.; Shi, Q.; Yan, L.; Geng, G.; Hong, C.; Li, M.; Liu, F.; Zheng, B.; Cao, J.; Ding, A.; Gao, J.; Fu, Q.; Huo, J.; Liu, B.; Liu, Z.; Yang, F.; He, K.; Hao, J., Drivers of improved $PM_{2.5}$ air quality in China from 2013 to 2017. *Proc. Natl. Acad. Sci. U. S. A.* **2019,** *116*, (49), 24463-24469.
34. Zhai, S.; Jacob, D. J.; Wang, X.; Shen, L.; Li, K.; Zhang, Y.; Gui, K.; Zhao, T.; Liao, H., Fine particulate matter ($PM_{2.5}$) trends in China, 2013–2018: separating contributions from anthropogenic emissions and meteorology. *Atmos. Chem. Phys.* **2019,** *19*, (16), 11031-11041.
35. Cai, J.; Wu, C.; Wang, J.; Du, W.; Zheng, F.; Hakala, S.; Fan, X.; Chu, B.; Yao, L.; Feng, Z.; Liu, Y.; Sun, Y.; Zheng, J.; Yan, C.; Bianchi, F.; Kulmala, M.; Mohr, C.; Daellenbach, K. R., Influence of organic aerosol composition determined by offline FIGAERO-CIMS on particle absorptive properties in autumn Beijing. *Atmos. Chem. Phys. Discuss.* **2021,** *2021*, 1-23.
36. Zhai, S.; Jacob, D. J.; Wang, X.; Liu, Z.; Wen, T.; Shah, V.; Li, K.; Moch, J. M.; Bates, K. H.; Song, S.; Shen, L.; Zhang, Y.; Luo, G.; Yu, F.; Sun, Y.; Wang, L.; Qi, M.; Tao, J.; Gui, K.; Xu, H.; Zhang, Q.; Zhao, T.; Wang, Y.; Lee, H. C.; Choi, H.; Liao, H., Control of particulate nitrate air pollution in China. *Nat. Geosci.* **2021,** *14*, 389–395.
37. Sun, Y. L.; Zhang, Q.; Schwab, J. J.; Demerjian, K. L.; Chen, W. N.; Bae, M. S.; Hung, H. M.; Hogrefe, O.; Frank, B.; Rattigan, O. V.; Lin, Y. C., Characterization of the sources and processes of organic and inorganic aerosols in New York city with a high-resolution time-of-flight aerosol mass apectrometer. *Atmos. Chem. Phys.* **2011,** *11*, (4), 1581-1602.
38. Wang, W. G.; Liu, M. Y.; Wang, T. T.; Song, Y.; Zhou, L.; Cao, J. J.; Hu, J. N.; Tang, G. G.; Chen, Z.; Li, Z. J.; Xu, Z. Y.; Peng, C.; Lian, C. F.; Chen, Y.; Pan, Y. P.; Zhang, Y. H.; Sun, Y. L.; Li, W. J.; Zhu, T.; Tian, H. Z.; Ge, M. F., Sulfate formation is dominated by manganese-catalyzed oxidation of SO_2 on aerosol surfaces during haze events. *Nat. Commun.* **2021,** *12*, (1), 1993-1993.

39. Sun, Y. L.; Du, W.; Fu, P. Q.; Wang, Q. Q.; Li, J.; Ge, X. L.; Zhang, Q.; Zhu, C. M.; Ren, L. J.; Xu, W. Q.; Zhao, J.; Han, T. T.; Worsnop, D. R.; Wang, Z. F., Primary and secondary aerosols in Beijing in winter: sources, variations and processes. *Atmos. Chem. Phys.* **2016,** *16*, (13), 8309-8329.
40. Chen, Q.; Liu, Y. J.; Donahue, N. M.; Shilling, J. E.; Martin, S. T., Particle-phase chemistry of secondary organic material: modeled compared to measured O:C and H:C elemental ratios provide constraints. *Environ. Sci. Technol.* **2011,** *45*, (11), 4763-4770.
41. Faust, J. A.; Wong, J. P. S.; Lee, A. K. Y.; Abbatt, J. P. D., Role of aerosol liquid water in secondary organic aerosol formation from volatile organic compounds. *Environ. Sci. Technol.* **2017,** *51*, (3), 1405-1413.
42. Riva, M.; Rantala, P.; Krechmer, J. E.; Perakyla, O.; Zhang, Y. J.; Heikkinen, L.; Garmash, O.; Yan, C.; Kulmala, M.; Worsnop, D.; Ehn, M., Evaluating the performance of five different chemical ionization techniques for detecting gaseous oxygenated organic species. *Atmos. Meas. Tech.* **2019,** *12*, (4), 2403-2421.
43. Hallquist, M.; Wenger, J. C.; Baltensperger, U.; Rudich, Y.; Simpson, D.; Claeys, M.; Dommen, J.; Donahue, N. M.; George, C.; Goldstein, A. H.; Hamilton, J. F.; Herrmann, H.; Hoffmann, T.; Iinuma, Y.; Jang, M.; Jenkin, M. E.; Jimenez, J. L.; Kiendler-Scharr, A.; Maenhaut, W.; McFiggans, G.; Mentel, T. F.; Monod, A.; Prevot, A. S. H.; Seinfeld, J. H.; Surratt, J. D.; Szmigielski, R.; Wildt, J., The formation, properties and impact of secondary organic aerosol: current and emerging issues. *Atmos. Chem. Phys.* **2009,** *9*, (14), 5155-5236.
44. Dai, W.-T.; Ho, S. S. H.; Ho, K.-F.; Cao, J.-J., Characterization of particulate-phase high molecular weight mono-carbonyls (C# > 5) and dicarbonyls in urban atmosphere of Xi'an, China. *Aerosol Air Qual. Res.* **2012,** *12*, (5), 892-901.
45. Donahue, N. M.; Epstein, S. A.; Pandis, S. N.; Robinson, A. L., A two-dimensional volatility basis set: 1. organic-aerosol mixing thermodynamics. *Atmos. Chem. Phys.* **2011,** *11*, (7), 3303-3318.
46. Xu, W.; Xie, C.; Karnezi, E.; Zhang, Q.; Wang, J.; Pandis, S. N.; Ge, X.; Wang, Q.; Zhao, J.; Du, W.; Qiu, Y.; Zhou, W.; He, Y.; Zhang, J.; An, J.; Li, Y.; Li, J.; Fu, P.; Wang, Z.; Worsnop, D. R.; Sun, Y., Summertime aerosol volatility measurements in Beijing, China. *Atmos. Chem. Phys.* **2019,** *19*, 10205-10216.
47. Bianchi, F.; Kurten, T.; Riva, M.; Mohr, C.; Rissanen, M. P.; Roldin, P.; Berndt, T.; Crounse, J. D.; Wennberg, P. O.; Mentel, T. F.; Wildt, J.; Junninen, H.; Jokinen, T.; Kulmala, M.; Worsnop, D. R.; Thornton, J. A.; Donahue, N. M.; Kjaergaard, H. G.; Ehn, M., Highly Oxygenated Organic Molecules (HOM) from gas-phase autoxidation involving peroxy radicals: a key contributor to atmospheric aerosol. *Chem. Rev.* **2019,** *119*, (6), 3472–3509.
48. Cheng, X.; Chen, Q.; Jie Li, Y.; Zheng, Y.; Liao, K.; Huang, G., Highly oxygenated organic molecules produced by the oxidation of benzene and toluene in a wide range of OH exposure and NOx conditions. *Atmos. Chem. Phys.* **2021,** *21*, (15), 12005-12019.
49. Gaston, C. J.; Lopez-Hilfiker, F. D.; Whybrew, L. E.; Hadley, O.; McNair, F.; Gao, H. L.; Jaffe, D. A.; Thornton, J. A., Online molecular characterization of fine particulate matter in Port Angeles, WA: Evidence for a major impact from residential wood smoke. *Atmos. Environ.* **2016,** *138*, 99-107.
50. Yan, C. Q.; Zheng, M.; Sullivan, A. P.; Shen, G. F.; Chen, Y. J.; Wang, S. X.; Zhao, B.; Cai, S. Y.; Desyaterik, Y.; Li, X. Y.; Zhou, T.; Gustafsson, O.; Collett, J. L., Residential coal combustion as a source of levoglucosan in China. *Environ. Sci. Technol.* **2018,** *52*, (3), 1665-1674.
51. Zhao, R.; Mungall, E. L.; Lee, A. K. Y.; Aljawhary, D.; Abbatt, J. P. D., Aqueous-phase photooxidation of levoglucosan - a mechanistic study using aerosol time-of-flight chemical ionization mass spectrometry (Aerosol ToF-CIMS). *Atmos. Chem. Phys.* **2014,** *14*, (18), 9695-9706.
52. Kawamura, K.; Bikkina, S., A review of dicarboxylic acids and related compounds in atmospheric aerosols: Molecular distributions, sources and transformation. *Atmos. Res.* **2016,** *170*, 140-160.
53. Zhao, W. Y.; Kawamura, K.; Yue, S. Y.; Wei, L. F.; Ren, H.; Yan, Y.; Kang, M. J.; Li, L. J.; Ren, L. J.; Lai, S. C.; Li, J.; Sun, Y. L.; Wang, Z. F.; Fu, P. Q., Molecular distribution and compound-specific stable carbon isotopic composition of dicarboxylic acids, oxocarboxylic acids and alpha-dicarbonyls in PM2.5 from Beijing, China. *Atmos. Chem. Phys.* **2018,** *18*, (4), 2749-2767.
54. Yu, Q.; Chen, J.; Qin, W. H.; Cheng, S. M.; Zhang, Y. P.; Ahmad, M.; Ouyang, W., Characteristics and secondary formation of water-soluble organic acids in PM_1, $PM_{2.5}$ and PM_{10} in Beijing during haze episodes. *Sci. Total Environ.* **2019,** *669*, 175-184.
55. Guo, H. Y.; Weber, R. J.; Nenes, A., High levels of ammonia do not raise fine particle pH sufficiently to yield nitrogen oxide-dominated sulfate production. *Sci Rep* **2017,** *7*, 12109.
56. Furukawa, T.; Takahashi, Y., Oxalate metal complexes in aerosol particles: implications for the hygroscopicity of oxalate-containing particles. *Atmos. Chem. Phys.* **2011,** *11*, (9), 4289-4301.
57. Ylisirnio, A.; Barreira, L. M. F.; Pullinen, I.; Buchholz, A.; Jayne, J.; Krechmer, J. E.; Worsnop, D. R.; Virtanen, A.; Schobesberger, S., On the calibration of FIGAERO-ToF-CIMS: importance and impact of calibrant delivery for the particle-phase calibration. *Atmos. Meas. Tech.* **2021,** *14*, (1), 355-367.
58. Paciga, A. L.; Riipinen, I.; Pandis, S. N., Effect of ammonia on the volatility of organic diacids. *Environ. Sci. Technol.* **2014,** *48*, (23), 13769-13775.
59. Carlton, A. G.; Wiedinmyer, C.; Kroll, J. H., A review of Secondary Organic Aerosol (SOA) formation from isoprene. *Atmos. Chem. Phys.* **2009,** *9*, (14), 4987-5005.
60. Zhao, R.; Lee, A. K. Y.; Abbatt, J. P. D., Investigation of aqueous-phase photooxidation of glyoxal and methylglyoxal by aerosol chemical ionization mass spectrometry: observation of hydroxyhydroperoxide formation. *J. Phys. Chem. A* **2012,** *116*, (24), 6253-6263.

61. Shen, H. Q.; Chen, Z. M.; Li, H.; Qian, X.; Qin, X.; Shi, W. X., Gas-particle partitioning of carbonyl compounds in the ambient atmosphere. *Environ. Sci. Technol.* **2018,** *52*, (19), 10997-11006.
62. Ortiz-Montalvo, D. L.; Hakkinen, S. A. K.; Schwier, A. N.; Lim, Y. B.; McNeill, V. F.; Turpin, B. J., Ammonium addition (and aerosol pH) has a dramatic impact on the volatility and yield of glyoxal secondary organic aerosol. *Environ. Sci. Technol.* **2014,** *48*, (1), 255-262.
63. Pavuluri, C. M.; Kawamura, K.; Mihalopoulos, N.; Swaminathan, T., Laboratory photochemical processing of aqueous aerosols: formation and degradation of dicarboxylic acids, oxocarboxylic acids and alpha-dicarbonyls. *Atmos. Chem. Phys.* **2015,** *15*, (14), 7999-8012.
64. Kautzman, K. E.; Surratt, J. D.; Chan, M. N.; Chan, A. W. H.; Hersey, S. P.; Chhabra, P. S.; Dalleska, N. F.; Wennberg, P. O.; Flagan, R. C.; Seinfeld, J. H., Chemical composition of gas- and aerosol-phase products from the photooxidation of naphthalene. *J. Phys. Chem. A.* **2010,** *114*, (2), 913-934.
65. Surratt, J. D.; Chan, A. W. H.; Eddingsaas, N. C.; Chan, M. N.; Loza, C. L.; Kwan, A. J.; Hersey, S. P.; Flagan, R. C.; Wennberg, P. O.; Seinfeld, J. H., Reactive intermediates revealed in secondary organic aerosol formation from isoprene. *Proc. Natl. Acad. Sci. U. S. A.* **2010,** *107*, (15), 6640-6645.
66. Sareen, N.; Schwier, A. N.; Shapiro, E. L.; Mitroo, D.; McNeill, V. F., Secondary organic material formed by methylglyoxal in aqueous aerosol mimics. *Atmos. Chem. Phys.* **2010,** *10*, (3), 997-1016.
67. Li, Y. X.; Ji, Y. M.; Zhao, J. Y.; Wang, Y.; Shi, Q. J.; Peng, J. F.; Wang, Y. Y.; Wang, C. Y.; Zhang, F.; Wang, Y. X.; Seinfeld, J. H.; Zhang, R. Y., Unexpected oligomerization of small α-dicarbonyls for secondary organic aerosol and brown carbon formation. *Environ. Sci. Technol.* **2021,** *55*, (8), 4430-4439.
68. Wang, Z. D.; Ehn, M.; Rissanen, M. P.; Garmash, O.; Quelever, L.; Xing, L.; Monge-Palacios, M.; Rantala, P.; Donahue, N. M.; Berndt, T.; Sarathy, S. M., Efficient alkane oxidation under combustion engine and atmospheric conditions. *Commun. Chem.* **2021,** *4*, 18.
69. Li, Y. X.; Zhao, J. Y.; Wang, Y.; Seinfeld, J. H.; Zhang, R. Y., Multigeneration production of secondary organic aerosol from toluene photooxidation. *Environ. Sci. Technol.* **2021,** *55*, (13), 8592-8603.
70. Wang, Y. J.; Hu, M.; Wang, Y. C.; Zheng, J.; Shang, D. J.; Yang, Y. D.; Liu, Y.; Li, X.; Tang, R. Z.; Zhu, W. F.; Du, Z. F.; Wu, Y. S.; Guo, S.; Wu, Z. J.; Lou, S. R.; Hallquist, M.; Yu, J. Z., The formation of nitro-aromatic compounds under high NOx and anthropogenic VOC conditions in urban Beijing, China. *Atmos. Chem. Phys.* **2019,** *19*, (11), 7649-7665.
71. Wang, L. W.; Wang, X. F.; Gu, R. R.; Wang, H.; Yao, L.; Wen, L.; Zhu, F. P.; Wang, W. H.; Xue, L. K.; Yang, L. X.; Lu, K. D.; Chen, J. M.; Wang, T.; Zhang, Y. H.; Wang, W. X., Observations of fine particulate nitrated phenols in four sites in northern China: concentrations, source apportionment, and secondary formation. Atmos. Chem. Phys. **2018,** *18*, (6), 4349-4359.
72. Liang, Y. H.; Wang, X. F.; Dong, S. W.; Liu, Z. Y.; Mu, J. S.; Lu, C. Y.; Zhang, J.; Li, M.; Xue, L. K.; Wang, W. X., Size distributions of nitrated phenols in winter at a coastal site in north China and the impacts from primary sources and secondary formation. *Chemosphere* **2020,** *250*, 9.
73. Li, X.; Wang, Y. J.; Hu, M.; Tan, T. Y.; Li, M. R.; Wu, Z. J.; Chen, S. Y.; Tang, X. Y., Characterizing chemical composition and light absorption of nitroaromatic compounds in the winter of Beijing. *Atmos. Environ.* **2020,** *237*, 117712.
74. Vidovic, K.; Jurkovic, D. L.; Sala, M.; Kroflic, A.; Grgic, I., Nighttime aqueous-phase formation of nitrocatechols in the atmospheric condensed phase. *Environ. Sci. Technol.* **2018,** *52*, (17), 9722-9730.
75. Roberts, J. M., The atmospheric chemistry of organic nitrates. *Atmos. Environ. Part a-General Topics* **1990,** *24*, (2), 243-287.
76. Rollins, A. W.; Browne, E. C.; Min, K. E.; Pusede, S. E.; Wooldridge, P. J.; Gentner, D. R.; Goldstein, A. H.; Liu, S.; Day, D. A.; Russell, L. M.; Cohen, R. C., Evidence for NOx control over nighttime SOA formation. *Science* **2012,** *337*, (6099), 1210-1212.
77. Huang, W.; Saathoff, H.; Shen, X. L.; Ramisetty, R.; Leisner, T.; Mohr, C., Chemical characterization of highly functionalized organonitrates contributing to night-time organic aerosol mass loadings and particle growth. *Environ. Sci. Technol.* **2019,** *53*, (3), 1165-1174.
78. Huang, W.; Yang, Y.; Wang, Y.; Gao, W.; Li, H.; Zhang, Y.; Li, J.; Zhao, S.; Yan, Y.; Ji, D.; Tang, G.; Liu, Z.; Wang, L.; Zhang, R.; Wang, Y., Exploring the inorganic and organic nitrate aerosol formation regimes at a suburban site on the North China Plain. *Sci. Total Environ.* **2021,** *768*, 144538.
79. Gao, K.; Zhang, Y.; Liu, Y.; Yang, M.; Zhu, T., Screening of imidazoles in atmospheric aerosol particles using a hybrid targeted and untargeted method based on ultra-performance liquid chromatography-quadrupole time-of-flight mass spectrometry. *Anal. Chim. Acta.* **2021,** *1163*, 338516.
80. Lee, B. H.; Mohr, C.; Lopez-Hilfiker, F. D.; Lutz, A.; Hallquist, M.; Lee, L.; Romer, P.; Cohen, R. C.; Iyer, S.; Kurten, T.; Hu, W. W.; Day, D. A.; Campuzano-Jost, P.; Jimenez, J. L.; Xu, L.; Ng, N. L.; Guo, H. Y.; Weber, R. J.; Wild, R. J.; Brown, S. S.; Koss, A.; de Gouw, J.; Olson, K.; Goldstein, A. H.; Seco, R.; Kim, S.; McAvey, K.; Shepson, P. B.; Starn, T.; Baumann, K.; Edgerton, E. S.; Liu, J. M.; Shilling, J. E.; Miller, D. O.; Brune, W.; Schobesberger, S.; D'Ambro, E. L.; Thornton, J. A., Highly functionalized organic nitrates in the southeast United States: Contribution to secondary organic aerosol and reactive nitrogen budgets. *Proc. Natl. Acad. Sci. U. S. A.* **2016,** *113*, (6), 1516-1521.
81. Tsiligiannis, E.; Hammes, J.; Salvador, C. M.; Mentel, T. F.; Hallquist, M., Effect of NOx on 1,3,5-trimethylbenzene (TMB) oxidation product distribution and particle formation. *Atmos. Chem. Phys.* **2019,** *19*, (23), 15073-15086.
82. Liu, S.; Shilling, J. E.; Song, C.; Hiranuma, N.; Zaveri, R. A.; Russell, L. M., Hydrolysis of organonitrate functional groups in aerosol particles. *Aerosol Sci. Technol.* **2012,** *46*, (12), 1359-1369.

83. Lim, Y. B.; Kim, H.; Kim, J. Y.; Turpin, B. J., Photochemical organonitrate formation in wet aerosols. *Atmos. Chem. Phys.* **2016,** *16*, (19), 12631-12647.
84. McNeill, V. F.; Woo, J. L.; Kim, D. D.; Schwier, A. N.; Wannell, N. J.; Sumner, A. J.; Barakat, J. M., Aqueous-phase secondary organic aerosol and organosulfate formation in atmospheric aerosols: A modeling study. *Environ. Sci. Technol.* **2012,** *46*, (15), 8075-8081.
85. Le Breton, M.; Wang, Y. J.; Hallquist, A. M.; Pathak, R. K.; Zheng, J.; Yang, Y. D.; Shang, D. J.; Glasius, M.; Bannan, T. J.; Liu, Q. Y.; Chan, C. K.; Percival, C. J.; Zhu, W. F.; Lou, S. R.; Topping, D.; Wang, Y. C.; Yu, J. Z.; Lu, K. D.; Guo, S.; Hu, M.; Hallquist, M., Online gas- and particle-phase measurements of organosulfates, organosulfonates and nitrooxy organosulfates in Beijing utilizing a FIGAERO ToF-CIMS. *Atmos. Chem. Phys.* **2018,** *18*, (14), 10355-10371.
86. Wang, Y. J.; Hu, M.; Guo, S.; Wang, Y. C.; Zheng, J.; Yang, Y. D.; Zhu, W. F.; Tang, R. Z.; Li, X.; Liu, Y.; Le Breton, M.; Du, Z. F.; Shang, D. J.; Wu, Y. S.; Wu, Z. J.; Song, Y.; Lou, S. R.; Hallquist, M.; Yu, J. Z., The secondary formation of organosulfates under interactions between biogenic emissions and anthropogenic pollutants in summer in Beijing. *Atmos. Chem. Phys.* **2018,** *18*, (14), 10693-10713.
87. Barnes, I.; Hjorth, J.; Mihalopoulos, N., Dimethyl sulfide and dimethyl sulfoxide and their oxidation in the atmosphere. *Chem. Rev.* **2006,** *106*, (3), 940-975.
88. Ge, X. L.; Zhang, Q.; Sun, Y. L.; Ruehl, C. R.; Setyan, A., Effect of aqueous-phase processing on aerosol chemistry and size distributions in Fresno, California, during wintertime. *Environ. Chem.* **2012,** *9*, (3), 221-235.
89. Yuan, H.; Wang, Y.; Zhuang, G. S., MSA in Beijing aerosol. *Chin. Sci. Bull.* **2004,** *49*, (10), 1020-1025.
90. Huang, S.; Poulain, L.; van Pinxteren, D.; van Pinxteren, M.; Wu, Z. J.; Herrmann, H.; Wiedensohler, A., Latitudinal and seasonal distribution of particulate MSA over the Atlantic using a validated quantification method with HR-ToF-AMS. *Environ. Sci. Technol.* **2017,** *51*, (1), 418-426.
91. Galloway, M. M.; Chhabra, P. S.; Chan, A. W. H.; Surratt, J. D.; Flagan, R. C.; Seinfeld, J. H.; Keutsch, F. N., Glyoxal uptake on ammonium sulphate seed aerosol: reaction products and reversibility of uptake under dark and irradiated conditions. *Atmos. Chem. Phys.* **2009,** *9*, (10), 3331-3345.
92. Aiken, A. C.; Decarlo, P. F.; Jimenez, J. L., Elemental analysis of organic species with electron ionization high-resolution mass spectrometry. *Anal. Chem.* **2007,** *79*, (21), 8350-8.

Table 1. Measured quantities correspond to the sampling period of daily filter samples analyzed by the FIGAERO I^--TOF-CIMS.

Daily filter category	Date	RH (%)	T (°C)	WS (m s^{-1})	$PM_{2.5}$ ($\mu g\ m^{-3}$) measured by TEOM	Main $PM_{2.5}$ components ($\mu g\ m^{-3}$) measured by TOF-ACSM					Major oxygenated organic compounds (ng m^{-3}) measured by FIGAERO I^--TOF-CIMS			
						Nitrate	Sulfate	MO-OOA	LO-OOA	POA	$C_6H_{10}O_5$ (levoglucosan)	$C_6H_5NO_3$ (nitrophenol)	$C_7H_7NO_3$ (methyl-nitrophenol)	$C_4H_6O_4$ (succinic acid)
Humid haze	12/28	64	-0.2	0.8	123.6	28.9	16.1	14.3	11.0	10.7	506.8	51.9	33.8	58.1
	12/29	74	-0.4	0.9	187.1	37.4	31.9	32.2	8.6	15.5	441.7	64.0	32.7	92.9
Dry haze	12/21	30	4.6	0.6	56.5	5.6	1.2	3.8	5.8	10.3	611.5	15.0	11.6	13.4
Clean	12/22	18	5.8	2.7	13.2	0.8	0.5	0.7	1.6	2.4	197.6	0.27	--[a]	0.54
	01/03	17	-2.3	4.3	13.8	0.6	1.1	0.4	2.4	1.4	82.9	0.55	--[a]	1.6
Transition	01/04	25	-2.9	1.9	25.3	1.7	1.2	1.0	3.3	3.7	397.7	3.8	3.3	6.2

[a]Signal intensities are lower than the detection limit.

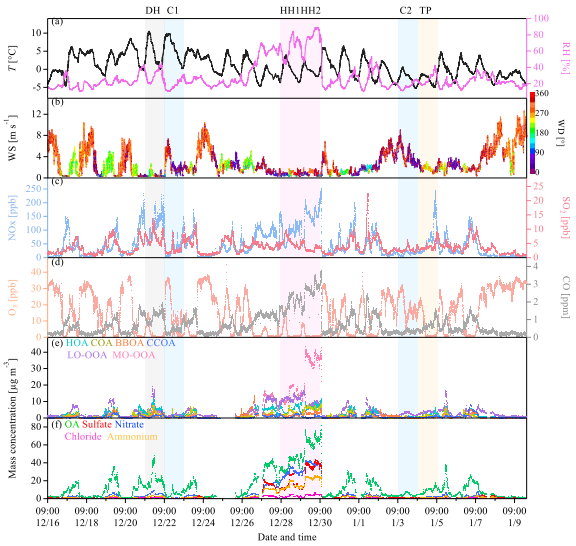

Figure 1. Time series of (a) T and RH, (b) WS colored by WD, (c) NO_x and SO_2, (d) O_3 and CO, (e, f) chemical composition of $PM_{2.5}$ in 2017. Case periods are selected as clean days (C1 and C2 for $PM_{2.5} < 15$ μg m^{-3}), dry haze (DH for $PM_{2.5} > 35$ μg m^{-3}, RH < 60%), humid haze (HH1 and HH2 for $PM_{2.5} > 35$ μg m^{-3}, RH > 60%), and transition period (TP for 15 μg $m^{-3} < PM_{2.5} < 35$ μg m^{-3}) (Table S1).

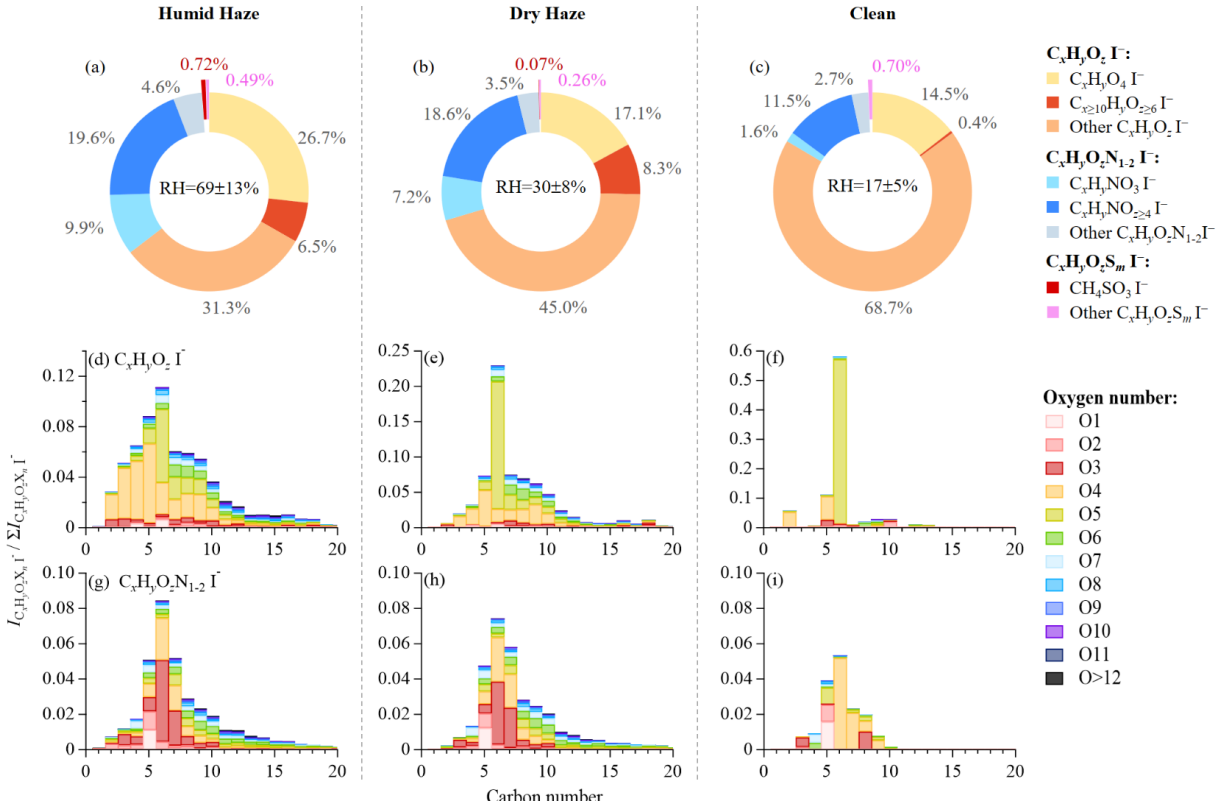

Figure 2. Signal intensity fraction of $C_xH_yO_z$, $C_xH_yO_zN_n$, and $C_xH_yO_zS_n$ compounds that cluster with I^- and stacked relative intensities of $C_xH_yO_z{\cdot}I^-$ and $C_xH_yO_zN_n{\cdot}I^-$ ions that are classified by carbon and oxygen numbers in their formulas for the (a, d, g) humid-haze, (b, e, h) dry-haze, and (c, f, i) clean-day cases.

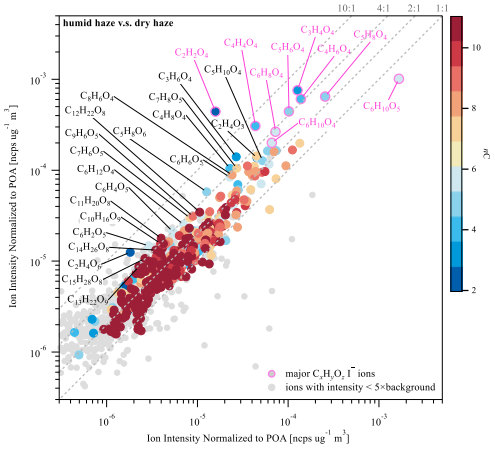

Figure 3. Scatter plot of the ion intensities of $C_xH_yO_z$ compounds normalized to the POA mass concentrations for the humid-haze and dry-haze cases. The data points were colored by the carbon number of their molecular formulas.

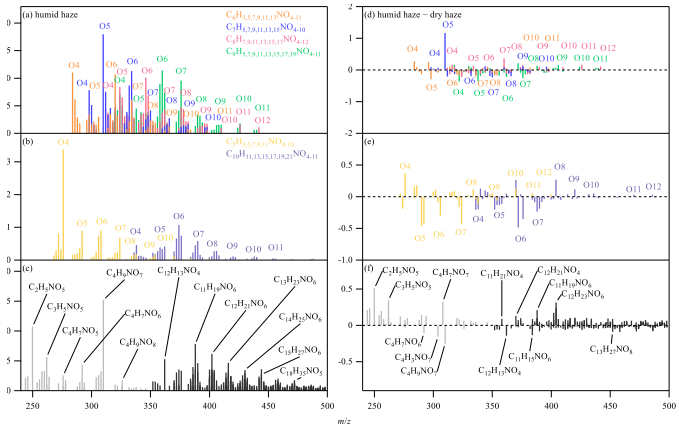

Figure 4. Mass contribution of individual ON molecules to total ONs and the difference between the humid-haze and dry-haze cases for (a, d) C_6, C_7, C_8, and C_9, (b, e) C_5 and C_{10}, and (c, f) other ion groups. I^- has been omitted in the molecular formulas of individual ions.

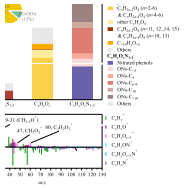

Figure 5. (a) Relative contribution of OOAs to the elevated SOA mass in $PM_{2.5}$ during the humid-haze (hh) compared with the dry-haze (dh) days and the corresponding molecular composition in mass fraction obtained by the online TOF-ACSM and the offline FIGAERO I^--TOF-CIMS measurements, respectively. The mass concentrations of OOAs were normalized to the POA concentrations to roughly account for the potential changes of atmospheric dilution given that the mean POA composition was similar for the two haze cases. (b) Mass spectral difference between MO-OOA and LO-OOA obtained by the LTOF-AMS measurements.

Supporting Information for

Precursors and pathways leading to enhanced secondary organic aerosol formation during severe haze episodes

Yan Zheng[1], Qi Chen[1,*], Xi Cheng[1], Claudia Mohr[2], Jing Cai[3], Wei Huang[3], Manish Shrivastava[4], Penglin Ye[5], Pingqing Fu[6], Xiaodi Shi[1], Yanli Ge[1], Keren Liao[1], Ruqian Miao[1], Xinghua Qiu[1], Theodore K. Koenig[1], Shiyi Chen[1]

[1]State Key Joint Laboratory of Environmental Simulation and Pollution Control, BIC-ESAT and IJRC, College of Environmental Sciences and Engineering, Peking University, Beijing 100871, China

[2]Department of Environmental Science and Analytical Chemistry, Stockholm University, Stockholm 11418, Sweden

[3]Institute for Atmospheric and Earth System Research, Faculty of Science, University of Helsinki, Helsinki 00014, Finland

[4]Pacific Northwest National Laboratory, Richland, Washington 99352, USA

[5]Shanghai Key Laboratory of Atmospheric Particle Pollution and Prevention, Department of Environmental Science and Engineering, Fudan University, Shanghai 200433, China

[6]Institute of Surface-Earth System Science, Tianjin University, Tianjin 300072, China

[*]*Correspondence to*: Qi Chen (email: qichenpku@pku.edu.cn)

This file includes:

Supporting text

Supporting Table S1-S5

Supporting Figure S1-S24

Supporting references

Number of pages: 38

Section A. Determination of the PMF solution and quantification of organic nitrates (ONs)

PMF analysis of $PM_{2.5}$ based on the data from the TOF-ACSM

PMF analysis was conducted on the organic mass spectra obtained from the TOF-ACSM by using the Igor PMF evaluation tool (PET, version 3.00B) (Paatero and Tapper, 1994;Ulbrich et al., 2009). The unit-mass-resolution (UMR) data between *m*/*z* 20 and 200 are used. A 6-factor solution was determined and the 6-factor solutions were tested in the PMF runs with various seed (0-50) and rotational parameter (f_{peak}) values. Seven or more factor solutions lead to clear splitting of the factors and therefore were not considered. The six statistical OA factors are labeled as more-oxidized oxygenated OA (MO-OOA), less-oxidized oxygenated OA (LO-OOA), hydrocarbon-like OA (HOA), and the OA factors possibly related to cooking (COA), biomass burning (BBOA), and coal combustion (CCOA). The TOF-ACSM sampled $PM_{2.5}$ for the first half of every hour and PM_1 for the rest half. Therefore, the organic spectra were analyzed by both a separate and a merged way for PM_1 and $PM_{2.5}$. The results from the two methods are well agreed with the Pearson's *R* greater than 0.98 and the discrepancies of ~2-19% (Figure S16 and S17). We adopted the results from the merged method for the discussions. Detailed information about the PMF analysis and the reasons of factor-solution choices are provided in Tables S4, S5 and Figure S18, S19, S20.

For the separate method, factor numbers from 1 to 8 were selected to run in the model and we ran PMF with a constant 6-factor for different fpeak values (-1 to 1, step by 0.2) and seed values (0-50). As indicated in Figure S18, only PMF solutions at fpeak -0.2, 0, 0.2 were converged. We compared the three sets of solutions and found that the solutions at fpeak -0.2 and 0 were nearly identical while the two types of OOA from solution at f_{peak} 0.2 were not well separated (Figure S19) and BBOA also demonstrated a certain mixing with CCOA. the time-series of four POA factors (HOA, COA, BBOA, and CCOA) were almost unchanged when f_{peak} values were changed. Moreover, the PMF solutions at all seed numbers were nearly identical to the final solution which was chosen in the manuscript (seed=0). Correlation coefficients (Pearson's *R*) of the six OA factors of $PM_{2.5}$ in 2017 winter of Beijing are listed in Table S5. MO-OOA is best correlated with all inorganic salts and is the only factor which is highly correlated with RH (R=0.86). LO-OOA does not show distinctively strong correlation with any external tracers. COA is well correlated with two maker ion for cooking activ ities ($C_5H_8O^+$ and $C_6H_{10}O^+$), distinguishing the COA factor from other factors. BBOA is best correlated with the tracer ion ($C_2H_4O_2^+$) of biomass burning. HOA shows good correlation with benzene, toluene, and NO_x. CCOA is best correlated with napthalene and PAHs. For the merged method, which is the same, factor numbers from 1 to 8 were run in the model. The model was also

run with 6-factor at different f_{peak} values (i.e., -1 to 1, stepped by 0.2) and seed values of 0-50. As indicated in Figure S20, the PMF solutions at f_{peak} other than 0 were not converged. Solutions at all seed numbers were nearly identical (Q=1.35886±0.00002).

Estimation of particulate ONs in PM_1 from the PMF method based on the AMS data

PMF analysis was performed based on the combined high-resolution (HR) organic and inorganic (NO^+ and NO_2^+ ions) matrix obtained from the AMS by using the Igor PMF evaluation tool (PET, version 3.00B) (Paatero and Tapper, 1994;Ulbrich et al., 2009;Sun et al., 2012;Xu et al., 2015). NO^+ and NO_2^+ could be fragmented from inorganic nitrate or organic nitrate, which could not be distinguised from the AMS data. Based on the PMF method, the NO^+ and NO_2^+ ions were allocated into a nitrate inorganic aerosol factor (NIA) and and other common OA factors (Figure S21, S22, S23). Similar to the classic PMF analysis based on the pure organic datasets previously performed by Zheng et al. (2020), the HR data between *m*/*z* 12 and 130 are used in the organic-inorganic mixed PMF analysis here. Nine factors were tested in the PMF runs with f_{peak} values (-1 to 1, step by 0.2) and seed numbers (0-50). A 7-factor solution was determined with the seed number and the f_{peak} value of zero. Eight or more factor solutions lead to clear splitting of the factors and therefore were not considered. The seven statistical OA factors include 6 common OA factors labeled as more-oxidized oxygenated OA (MO-OOA), less-oxidized oxygenated OA (LO-OOA), hydrocarbon-like OA (HOA), cooking (COA), biomass burning (BBOA), coal combustion (CCOA) and a NIA factor. Details of the 6 OA factors from the classic PMF method were described by Zheng et al. (2020) For the rotation and seed test, the 7-factor solutions were converged at f_{peak} of 0, 0.4 and 0.6 with similar results while solutions at seed 1-4, 6, 10, 12, 15, 17, 19, 25, 34, 43, 46, 47, and 49 are not well separated with some mixing of HOA, CCOA, and LO-OOA.

The NO^+ and NO_2^+ ions in the OA factors ($[NO^+_{org}]$ and $[NO^+_{2,org}]$) are mainly contributed from nitrate-containing organic compounds, which could be calculated following eq1 and eq2 adopted from Xu et al. (2015):

$$\left[NO^+_{org}\right] = \sum \left([\text{OA factor}]_i \times f_{NO,i}\right) \qquad (1)$$

$$\left[NO^+_{2,org}\right] = \sum \left([\text{OA factor}]_i \times f_{NO2,i}\right) \qquad (2)$$

Where $[\text{OA factor}]_i$ is the mass concentration of each OA factor; $f_{NO_2,i}$and $f_{NO,i}$ represent the relative contribution of NO^+ and NO_2^+ ions in the i^{th} OA factor. Here we only used the sum of $\left[NO^+_{org}\right]_{SOA}$ and $\left[NO^+_{org}\right]_{SOA}$ to estimated the total particulate ONs considering that ONs are mainly secondary products the OH•-induced oxidation under high-NO_x conditions or NO_3•-initiated oxidation during nighttime (Roberts, 1990;Ng et al., 2017). An average molecular weight (MW) of 231.4, 220.1, and 184.2 g mol^{-1} was applied for humid-haze, dry-haze, and clean-day

samples respectively based on the average formula of ONs obtained from the FIGAERO I^- CIMS ($C_{8.9}H_{14.6}O_6N_1$, $C_9H_{15.1}O_6N_1$, and $C_{6.2}H_{9.4}O_{5.4}N_1$, respectively). These values are similar to the average molecular weight of 200~300 g mol^{-1} for organic nitrates from biogenic VOCs (Surratt et al., 2008;Rollins et al., 2012). The correction of relative ionization efficiency (RIE) differences between OA and inorganic nitrate (mainly ammonium nitrate) was also applied to obtain the mass concentrations of ONs following eq3. The RIE vaues of 1.1 and 1.4 are applied for ammonium nitrate (RIE_{NO3}) and OA (RIE_{org}) respectively, which are commonly used default values for AMS (Canagaratna et al., 2007).

$$[\mathrm{ONs}] = \left(\frac{[NO^+_{org}]}{30} + \frac{[NO^+_{2,org}]}{46} \right) \times MW \times \frac{RIE_{NO3}}{RIE_{org}} \qquad (3)$$

Section B. Classification of the filter samples for the offline FIGAERO I^--TOF-CIMS measurements

As shown in Table S1, the filter samples were classified into four groups (clean, transition, dry haze, and humid haze) based on the daily mean $PM_{2.5}$ concentrations and RH: clean ($PM_{2.5}$ < 15 μg m^{-3}), dry haze ($PM_{2.5}$ > 35 μg m^{-3}, RH < 60%), humid haze ($PM_{2.5}$ > 35 μg m^{-3}, RH > 60%), and transition (15 < $PM_{2.5}$ < 35 μg m^{-3}). The standards of $PM_{2.5}$ for pollution (35 μg m^{-3}) and clean period (15 μg m^{-3}) are respectively the national standards for daily mean and annual mean concentration of total $PM_{2.5}$. The RH of 60% was chosen to indicate humid haze cases for the following reasons. First, severe winter haze events in NCP are typically associated with high RH. Second, a previous study in Beijing winter which has similar chemical compositions to our study indicates that particles are plausibly in the liquid phase when RH increases over 60%. The RH in winter in Beijing is typically lower than 40%.

With this criteria, 3 “humid haze” samples, 3 “dry haze” samples, 3 “clean” samples, and 6 “transition” samples were classified. Among these samples, two “humid haze” (YY/MM/DD, 17/12/28 and 17/12/29), two “clean” (17/12/22, 18/01/03), one “dry haze” (17/12/21), and one “transition” (18/01/04) samples were chosen for the offline FIGAERO analysis. The sample on 17/12/27 was not chosen as a good example of “humid haze” because the severe haze evolution started on the day. The sample on 17/12/24 was not selected due to the limited data coverage (50% of the day) for the online chemical compositions of $PM_{2.5}$. For “dry haze” cases, the days 17/12/31 and 18/01/01 were not chosen as good examples because they were right after the severe humid haze event. The pollution moves regionally back and forth depending on the wind strength and the particle composition might be affected by the previous humid haze event.

Generally, the selected six days could provide solid information on the OA molecular composition for the following reasons: (1) the three parallel samples agree well on the mass spectra (Figure S24); (2) the total signal intensities of $C_xH_yO_zX_n \cdot I^-$ of the filter samples correlate well with the daily-mean OOA mass concentrations (R = 0.96) (Figure S9 in the SI); and (3) our results agree with a separate study using offline FIGAERO I^--TOF-CIMS in winter in 2018 in Beijing (Cai et al., 2021, ACPD) (Figure S11 in the SI).

Section C. Estimation of the aerosol liquid water content (ALWC)

The ALWC contributed from major inorganic components (ammonium, sulfate, nitrate, and chloride, $ALWC_{inorg}$) was estimated by a thermodynamic model ISORROPIA-II (Fountoukis and Nenes, 2007). The reverse mode with the assumption of metastable state was applied. The contribution of organic components to ALWC was estimated by the following eq4 (Petters and Kreidenweis, 2007;Nguyen et al., 2016),

$$ALWC_{org} = \frac{\kappa_{org} m_{org} \rho_{water} RH}{\rho_{org}(1\text{-}RH)} \quad (4)$$

where κ_{org} is the hygroscopicity parameter of OA, m_{org} refers to the mass concentration of OA (μg m^{-3}), ρ_{org} and ρ_{water} respectively refer to the average density of OA and pure water. A single κ_{org} of 0.1 was applied for the whole campaign considering that it is close to the reported values of κ for urban environments and OA has a relatively minor contribution compared to inorganic salts (Nguyen et al., 2016;Liu et al., 2019). In this study, assuming a κ_{org} of 0.1 results in ~15% of aerosol water from OA. The total ALWC is the sum of $ALWC_{inorg}$ and $ALWC_{org}$.

References

Bannan, T. J., Le Breton, M., Priestley, M., Worrall, S. D., Bacak, A., Marsden, N. A., Mehra, A., Hammes, J., Hallquist, M., Alfarra, M. R., Krieger, U. K., Reid, J. P., Jayne, J., Robinson, W., McFiggans, G., Coe, H., Percival, C. J., and Topping, D.: A method for extracting calibrated volatility information from the FIGAERO-HR-ToF-CIMS and its experimental application, Atmos. Meas. Tech., 12, 1429-1439, 10.5194/amt-12-1429-2019, 2019.

Cai, J., Wu, C., Wang, J., Du, W., Zheng, F., Hakala, S., Fan, X., Chu, B., Yao, L., Feng, Z., Liu, Y., Sun, Y., Zheng, J., Yan, C., Bianchi, F., Kulmala, M., Mohr, C., and Daellenbach, K. R.: Influence of organic aerosol composition determined by offline FIGAERO-CIMS on particle absorptive properties in autumn Beijing, Atmos. Chem. Phys. Discuss., 2021, 1-23, 10.5194/acp-2021-528, 2021.

Canagaratna, M. R., Jayne, J. T., Jimenez, J. L., Allan, J. D., Alfarra, M. R., Zhang, Q., Onasch, T. B., Drewnick, F., Coe, H., and Middlebrook, A.: Chemical and microphysical characterization of ambient aerosols with the aerodyne aerosol mass spectrometer, Mass Spectrom. Rev., 26, 185-222, 2007.

Fountoukis, C., and Nenes, A.: ISORROPIA II: a computationally efficient thermodynamic equilibrium model for K+-Ca2+-Mg2+-Nh(4)(+)-Na+-SO42--NO3--Cl--H2O aerosols, Atmos. Chem. Phys., 7, 4639-4659, 10.5194/acp-7-4639-2007, 2007.

Lee, B. H., Lopez-Hilfiker, F. D., Mohr, C., Kurten, T., Worsnop, D. R., and Thornton, J. A.: An Iodide-Adduct High-Resolution Time-of-Flight Chemical-Ionization Mass Spectrometer: Application to Atmospheric Inorganic and Organic Compounds, Environ. Sci. Technol., 48, 6309-6317, 10.1021/es500362a, 2014.

Liu, Y. C., Wu, Z. J., Huang, X. F., Shen, H. Y., Bai, Y., Qiao, K., Meng, X. X. Y., Hu, W. W., Tang, M. J., and He, L. Y.: Aerosol Phase State and Its Link to Chemical Composition and Liquid Water Content in a Subtropical Coastal Megacity, Environ. Sci. Technol., 53, 5027-5033, 10.1021/acs.est.9b01196, 2019.

Lopez-Hilfiker, F. D., Mohr, C., Ehn, M., Rubach, F., Kleist, E., Wildt, J., Mentel, T. F., Lutz, A., Hallquist, M., Worsnop, D., and Thornton, J. A.: A novel method for online analysis of gas and particle composition: description and evaluation of a Filter Inlet for Gases and AEROsols (FIGAERO), Atmos. Meas. Tech., 7, 983-1001, 10.5194/amt-7-983-2014, 2014.

Ng, N. L., Brown, S. S., Archibald, A. T., Atlas, E., Cohen, R. C., Crowley, J. N., Day, D. A., Donahue, N. M., Fry, J. L., Fuchs, H., Griffin, R. J., Guzman, M. I., Herrmann, H., Hodzic, A., Iinuma, Y., Jimenez, J. L., Kiendler-Scharr, A., Lee, B. H., Luecken, D. J., Mao, J. Q., McLaren, R., Mutzel, A., Osthoff, H. D., Ouyang, B., Picquet-Varrault, B., Platt, U., Pye, H. O. T., Rudich, Y., Schwantes, R. H., Shiraiwa, M., Stutz, J., Thornton, J. A., Tilgner, A., Williams, B. J., and Zaveri, R. A.: Nitrate radicals and biogenic volatile organic compounds: oxidation, mechanisms, and organic aerosol, Atmos. Chem. Phys., 17, 2103-2162, 10.5194/acp-17-2103-2017, 2017.

Nguyen, T. K. V., Zhang, Q., Jimenez, J. L., Pike, M., and Carlton, A. G.: Liquid Water: Ubiquitous Contributor to Aerosol Mass, Environ. Sci. Technol. Lett., 3, 257-263, 10.1021/acs.estlett.6b00167, 2016.

Paatero, P., and Tapper, U.: Positive Matrix Factorization - A nonnegative factor model with optimal utilization of error-estimates of data values, Environmetrics, 5, 111-126, 10.1002/env.3170050203, 1994.

Petters, M. D., and Kreidenweis, S. M.: A single parameter representation of hygroscopic growth and cloud condensation nucleus activity, Atmos. Chem. Phys., 7, 1961-1971, 10.5194/acp-7-1961-2007, 2007.

Roberts, J. M.: THE ATMOSPHERIC CHEMISTRY OF ORGANIC NITRATES, Atmospheric Environment Part a-General Topics, 24, 243-287, 10.1016/0960-1686(90)90108-y, 1990.

Rollins, A. W., Browne, E. C., Min, K. E., Pusede, S. E., Wooldridge, P. J., Gentner, D. R., Goldstein, A. H., Liu, S., Day, D. A., Russell, L. M., and Cohen, R. C.: Evidence for NOx Control over Nighttime SOA Formation, Science, 337, 1210-1212, 10.1126/science.1221520, 2012.

Serjeant, E. P., and Dempsey, B.: Ionization Constants of Organic Acids in Aqueous Solution, Pergamon, Oxford, 1979.

Shi, X. D., Qiu, X. H., Cheng, Z., Chen, Q., Rudich, Y., and Zhu, T.: Isomeric Identification of Particle-Phase Organic Nitrates through Gas Chromatography and Time-of-Flight Mass Spectrometry Coupled with an Electron Capture Negative Ionization Source, Environ. Sci. Technol., 54, 707-713, 10.1021/acs.est.9b05818, 2020.

Sun, Y. L., Zhang, Q., Schwab, J. J., Yang, T., Ng, N. L., and Demerjian, K. L.: Factor analysis of combined organic and inorganic aerosol mass spectra from high resolution aerosol mass spectrometer measurements, Atmos. Chem. Phys., 12, 8537-8551, 10.5194/acp-12-8537-2012, 2012.

Surratt, J. D., Gomez-Gonzalez, Y., Chan, A. W. H., Vermeylen, R., Shahgholi, M., Kleindienst, T. E., Edney, E. O., Offenberg, J. H., Lewandowski, M., Jaoui, M., Maenhaut, W., Claeys, M., Flagan, R. C., and Seinfeld, J. H.: Organosulfate formation in biogenic secondary organic aerosol, J. Phys. Chem. A, 112, 8345-8378, 10.1021/jp802310p, 2008.

Ulbrich, I. M., Canagaratna, M. R., Zhang, Q., Worsnop, D. R., and Jimenez, J. L.: Interpretation of organic components from Positive Matrix Factorization of aerosol mass spectrometric data, Atmos. Chem. Phys., 9, 2891-2918, 10.5194/acp-9-2891-2009, 2009.

Xu, L., Suresh, S., Guo, H., Weber, R. J., and Ng, N. L.: Aerosol characterization over the southeastern United States using high-resolution aerosol mass spectrometry: spatial and seasonal variation of aerosol composition and sources with a focus on organic nitrates, Atmos. Chem. Phys., 15, 7307-7336, 10.5194/acp-15-7307-2015, 2015.

Zheng, Y., Cheng, X., Liao, K., Li, Y., Li, Y. J., Huang, R. J., Hu, W., Liu, Y., Zhu, T., Chen, S., Zeng, L., Worsnop, D. R., and Chen, Q.: Characterization of anthropogenic organic aerosols by TOF-ACSM with the new capture vaporizer, Atmos. Meas. Tech., 13, 2457-2472, 10.5194/amt-13-2457-2020, 2020.

Table S1. The daily mean and one standard deviation of the meteorological parameters, the total mass loading of $PM_{2.5}$ measured by TEOM, and the non-refractory chemical composition of $PM_{2.5}$ measured by TOF-ACSM corresponding to the filter sampling periods.

Date	Filter	RH	T	WS	$PM_{2.5}$	Major $PM_{2.5}$ components ($\mu g\ m^{-3}$)						
(9AM-9AM)	Category	(%)	(°C)	($m\ s^{-1}$)	($\mu g\ m^{-3}$)	Nitrate	Sulfate	Ammonium	MO-OOA	LO-OOA	POA	ALWC
2017.12.21	Dry haze	30.3±7.5	4.6±3.3	0.6±0.5	56.5±20.1	5.6±1.6	1.2±0.3	2.5±0.7	3.8±1.0	5.8±4.2	10.3±4.7	1.9±1.0
2017.12.22	Clean	17.6±5.8	5.8±3.2	2.7±1.9	13.2±8.2	0.8±0.4	0.5±0.1	0.5±0.3	0.7±0.5	1.6±0.5	2.4±2.0	0.2±0.2
2017.12.23	Transition	24.7±3.3	4.2±1.1	3.1±2.3	31.3±14.4	2.5±1.4	1.4±0.7	1.4±0.4	1.3±0.9	3.7±1.6	4.9±3.9	0.8±0.3
2017.12.24	Clean*	18.2±2.3	0.9±2.1	4.6±2.7	7.4±6.2	0.3±0.1	0.7±0.1	0.3±0.2	0.1±0.1	1.0±0.6	0.5±0.4	0.2±0.04
2017.12.25	Transition	21.4±3.8	1.2±2.1	2.4±1.0	33.5±19.4	-	-	-	-	-	-	-
2017.12.26	Transition	37.7±14.9	0.5±3.1	2.3±1.0	34.4±17.1	3.8±1.6	1.3±0.5	1.9±0.8	2.2±1.6	3.4±1.7	7.2±4.3	2.5±2.3
2017.12.27	Humid haze	61.8±4.1	-1.5±1.2	1.4±0.9	93.0±17.3	15.3±2.7	14.0±4.1	9.6±1.8	11.7±3.2	9.0±2.6	10.2±2.8	29.7±7.1
2017.12.28	Humid haze	64.1±12.1	-0.2±2.2	0.8±0.4	123.6±25.4	28.9±4.1	16.1±6.0	14.2±3.3	14.3±3.6	11.0±1.2	10.7±3.3	57.2±39.5
2017.12.29	Humid haze	73.8±12.8	-0.4±1.3	0.9±0.4	187.1±39.1	37.4±4.3	31.9±10.5	21.3±4.4	32.2±9.4	8.6±3.2	15.5±3.3	143.6±91.7
2017.12.30	Transition	24.9±16.7	1.9±2.5	1.9±1.4	33.5±65.2	3.8±10.8	4.2±10.6	2.5±6.6	4.1±11.2	1.5±1.2	3.4±6.3	9.2±32.1
2017.12.31	Dry haze	24.4±7.1	1.2±3.1	1.0±0.4	39.8±19.1	3.7±1.3	2.2±0.7	2.1±0.7	3.2±1.5	4.8±2.4	7.2±4.4	1.3±0.8
2018.01.01	Dry haze	29.2±13.3	0.2±2.9	1.8±0.6	42.5±22.6	3.2±1.6	1.7±0.9	1.9±1.0	2.4±1.3	4.8±2.5	6.0±3.6	2.1±1.6
2018.01.02	Transition	19.0±5.0	-1.0±2.3	4.7±1.6	15.1±11.1	0.7±0.7	1.0±0.3	0.6±0.3	0.5±0.5	1.4±0.7	2.0±1.1	0.3±0.2
2018.01.03	Clean	17.1±4.2	-2.3±1.6	4.3±2.0	13.8±6.2	0.6±0.2	1.1±0.1	0.6±0.1	0.4±0.2	2.4±0.8	1.4±0.7	0.3±0.1
2018.01.04	Transition	25.3±6.4	-2.9±1.2	1.9±0.8	25.3±12.2	1.7±0.6	1.2±0.1	1.1±0.3	1.0±0.5	3.3±0.7	3.7±2.2	0.8±0.5

*The online data from TOF-ACSM on 2017.12.24 covered 50% of the day.

Table S2. Sensitivity per million total reagent ion cps.

Formula	Observed formula	Nominated compounds	Sensitivity (cps ppt^{-1})	
			this study (IMR~200 mbar)	Lee et al. (2014) (IMR~100 mbar)
CH_2O_2	$CH_2O_2\ I^-$	Formic acid	10.8	2.9±0.6
$C_2H_2O_4$	$C_2H_2O_4\ I^-$	Oxalic acid	47.2	0.21±0.09
$C_3H_4O_4$	$C_3H_4O_4\ I^-$	Malonic acid	--	19±4.5
$C_4H_6O_4$	$C_4H_6O_4\ I^-$	Succinic acid	74.4	18±7.3
$C_5H_8O_4$	$C_5H_8O_4\ I^-$	Glutaric acid	77.8	15±5.6
$C_8H_6O_4$	$C_8H_6O_4\ I^-$	Phthalic acid	19.7	4.5±1.9
$C_6H_{10}O_5$	$C_6H_{10}O_5\ I^-$	Levoglucosan	27.1	--
$C_6H_5NO_3$	$C_6H_5NO_3\ I^-$	4-nitrophenol	183.3	--
$C_7H_7NO_3$	$C_7H_7NO_3\ I^-$	2-methyl-4-nitrophenol	145.5	--
$C_8H_9NO_4$	$C_8H_9NO_4\ I^-$	1-hydroxy-2-nitrooxyethyl benzene	8.3[a]	--
$C_7H_{15}NO_4$	$C_7H_{15}NO_4\ I^-$	nitrooxy-heptanol	8.0[a]	--
$C_8H_{17}NO_4$	$C_8H_{17}NO_4\ I^-$	nitrooxy-octanol	9.8[a]	--
$C_8H_9NO_3$	$C_8H_9NO_3\ I^-$	Phenyl nitrate	not detected	--
$C_7H_{15}NO_3$	$C_7H_{15}NO_3\ I^-$	Heptyl nitrate	not detected	--

[a]The purities of the synthesized organic nitrates are 54% for $C_8H_9NO_4$, 72% for $C_7H_{15}NO_4$, and 71% for $C_8H_{17}NO_4$, which are corrected in the sensitivity calibration (Shi et al., 2020);

Table S3. Dissociation constants (pK_{a1} and pK_{a2}) of acids and desorption temperatures corresponding to the maximum signal intensities (T_{max}) in the thermogram obtained by the FIGAERO I$^-$-ToF-CIMS. The pK_a values are obtained from Serjeant and Dempsey (1979).

Formula	Tentatively Assigned Species Name	pK_{a1}	pK_{a2}	T_{max} ± 1σ (°C) Lab standards			Ambient
				Lopez-Hilfiker et al. (2014)	Bannan et al. (2019)	This study	This study[c]
CH_4SO_3	Methanesulfonic acid	1.86	--	--	--	--	143.7±0.3
$C_2H_2O_4$	Oxalic Acid	1.25	3.81	--	--	38.3±3.7	143.2±0.7
$C_3H_4O_4$	Malonic Acid	2.85	5.70	--	58.4[a]; 67.5[b]	--	105.0±1.8
$C_4H_6O_4$	Succinic Acid	4.21	5.64	--	62.1[a]; 69.1[b]	66.8±4.0	77.4±0.7
$C_5H_8O_4$	Glutaric Acid	4.32	5.42	--	88.3[a]; 77.8[b]	55.0±3.4	73.6±1.2
$C_6H_{10}O_4$	Adipic Acid	4.41	5.41	--	102.3[a]; 103.0[b]	71.9±2.7	76.3±1.8
$C_7H_{12}O_4$	Pimelic Acid	4.71	5.58	--	89.6[b]	--	80.4±4.1
$C_8H_{14}O_4$	Suberic Acid	4.52	-	--	120.3[a]	--	81.8±1.4
$C_9H_{16}O_4$	Azelaic Acid	4.53	5.33	71.4[a]	--	--	92.6±1.3
$C_{10}H_{18}O_4$	Sebacic Acid	4.59	5.59	72.9[a]	--	--	92.6±1.6
$C_4H_4O_4$	Maleic Acid	1.92	6.23	--	--	--	99.6±0.7
	Fumaric Acid	3.02	4.38			--	
$C_5H_6O_4$	1,1-Cyclopropane-diacid	1.82	7.43	--	--	--	87.9±5.9
	trans-1-Propene-1,2-diacid	3.09	4.75			--	
	1-Propene-2,3-diacid	3.85	5.45			--	
$C_9H_{14}O_4$	Pinic Acid	--	--	61.5[a]	114.2[a]	--	84.4±3.9

[a]Based on pure compounds;

[b]Based on chamber SOA mixtures for which isomers may exist;

[c]Data from the humid haze.

Table S4. Detailed descriptions of the PMF solutions of $PM_{2.5}$ based on by the separated-matrix.

Factor Number	**Fpeak**	**Seed**	Q/Q_{exp}	**Solution Description**
1	0	0	7.37	Too few factors and large residuals
2	0	0	4.51	Too few factors. Q/Q_{exp} substantially decreases (39% of the maximum Q) but there still exist large residuals at time periods and key m/z. One of the two factors is POA-like while another is OOA-like.
3	0	0	3.01	Too few factors. Q/Q_{exp} substantially decreases (20-% of the maximum Q) but there still exist large residuals at time periods and key m/z. Two factors are POA-like and one is OOA-like.
4	0	0	2.19	Q/Q_{exp} still decreases very fast (11% of the maximum Q). The four factors are respectively CCOA-like, OOA-like, COA-like, and HOA-OOA mixed. More factors are needed.
5	0	0	1.76	Q/Q_{exp} decreases by 6% of the maximum Q. A new OOA factor is separated and therefore we identify two OOA factors, LO-OOA and MO-OOA. Except for LO-OOA, MO-OOA, and COA, the characteristic of the other three typical fossil-fuel-combustion factors (HOA, BBOA, and CCOA) are not clear, indicating certain mixing effects.
6	**0**	**0**	**1.45**	**Optimum choices for PMF factors (MO-OOA, LO-OOA, HOA, COA, CCOA and BBOA). Time series and diurnal variations of PMF factors are consistent with the external tracers.**
7-8	0	0	1.30-1.21	Q/Q_{exp} decreases little (<2% of the maximum Q). Factors split, e.g., HOA and CCOA

Table S5. Correlation coefficients (Pearson's *R*) of the six OA factors in $PM_{2.5}$ by the separated-matrix method with external tracers, including gas and aerosol species, meterology parameters. The top-five values of each OA factor are bold.

name	MO-OOA	LO-OOA	COA	BBOA	HOA	CCOA
Acetaldehyde	0.68	0.70	**0.91**	**0.62**	**0.91**	0.43
Acetone	0.83	**0.72**	0.84	0.58	0.90	0.44
Acetonitrile	0.17	0.56	0.71	0.53	0.81	0.50
Ammonium	**0.97**	0.68	0.74	0.45	0.71	0.17
Benzene	0.85	**0.72**	0.88	**0.63**	**0.95**	0.54
BP	0.06	-0.10	-0.09	0.04	-0.09	-0.12
$C_2H_4O_2^+$	0.17	**0.73**	**0.89**	**0.64**	**0.95**	**0.62**
$C_5H_8O^+$	0.50	**0.71**	**0.95**	0.55	0.83	0.39
$C_6H_{10}O^+$	0.79	0.65	**0.91**	0.50	0.76	0.37
Chloride	**0.94**	0.70	0.79	0.55	0.82	0.34
CO	**0.86**	0.68	0.86	0.57	0.90	0.47
Naphthalene	0.75	0.60	0.78	**0.63**	**0.93**	**0.70**
Nitrate	**0.94**	**0.73**	0.74	0.45	0.72	0.19
NO	0.63	0.38	0.71	0.47	0.82	0.54
NO_2	0.62	0.65	0.82	0.58	0.82	0.49
NOx	0.67	0.50	0.79	0.54	0.87	**0.56**
O_3	-0.43	-0.54	-0.66	-0.48	-0.72	-0.53
Ox	0.72	0.58	0.79	0.54	0.68	0.20
PAHs	0.62	0.35	0.47	0.46	0.67	**0.63**
RH	0.86	0.65	0.66	0.48	0.76	0.30
SO_2	0.13	0.51	0.43	0.43	0.55	**0.60**
Sulfate	**0.98**	0.56	0.70	0.40	0.64	0.10
Temperature	-0.25	-0.14	-0.17	-0.23	-0.24	-0.27
Toluene	0.84	0.68	**0.89**	**0.65**	**0.92**	0.50
WS	-0.33	-0.42	-0.50	-0.32	-0.53	-0.34

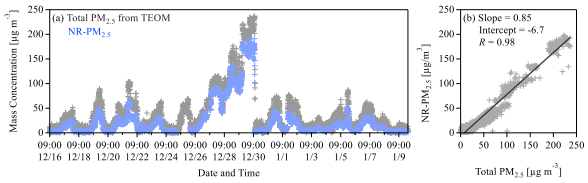

Figure S1. (a) Time series of the concentrations of NR-$PM_{2.5}$ measured by the ToF-ACSM and total $PM_{2.5}$ measured by the TEOM; (b) Scatter plot of NR-$PM_{2.5}$ versus total $PM_{2.5}$. The slope and the correlation coefficient (Pearson's *R*) are obtained by the orthogonal distance regression with intercepts.

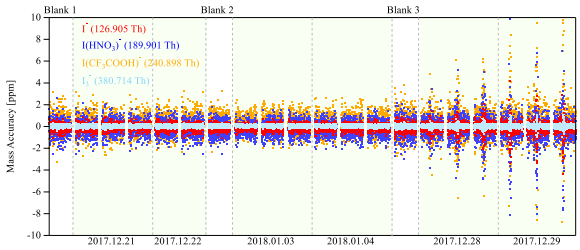

Figure S2. Time series of the mass accuracy of I^-, $I(HNO_3)^-$, $I(CF_3COOH)^-$, and I_3^- for all samples.

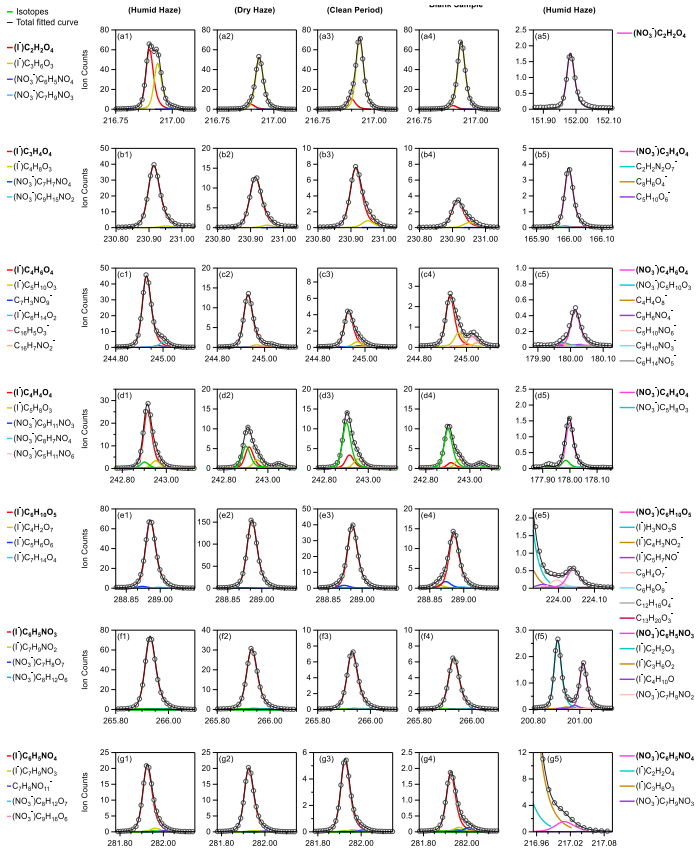
Isotopes
Total fitted curve
(Humid Haze)
(Dry Haze)
(Clean Period)
(Humid Haze)
Ion Counts
(a1)
(a2)
(a3)
(a4)
(a5)
(b1)
(b2)
(b3)
(b4)
(b5)
(c1)
(c2)
(c3)
(c4)
(c5)
(d1)
(d2)
(d3)
(d4)
(d5)
(e1)
(e2)
(e3)
(e4)
(e5)
(f1)
(f2)
(f3)
(f4)
(f5)
(g1)
(g2)
(g3)
(g4)
(g5)

(Continued)

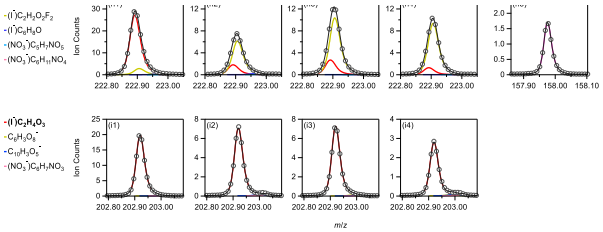

Figure S3. High-resolution peak fitting of major ions in the average mass spectra obtained by I^--TOF-CIMS.

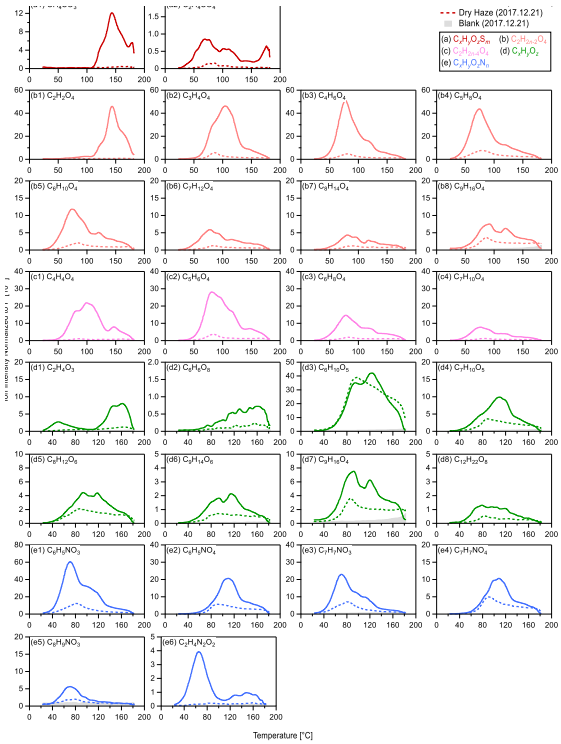

Figure S4. The thermograms of selected major ions from five categories: (a) $C_xH_yO_zS_m$ I^-, (b) $C_nH_{2n-2}O_4$ I^-, (c) $C_nH_{2n-4}O_4$ I^-, (d) other $C_xH_yO_z$ I^-, (e) $C_xH_yO_zN_n$ I^-. Formulas of the corresponding molecules are shown.

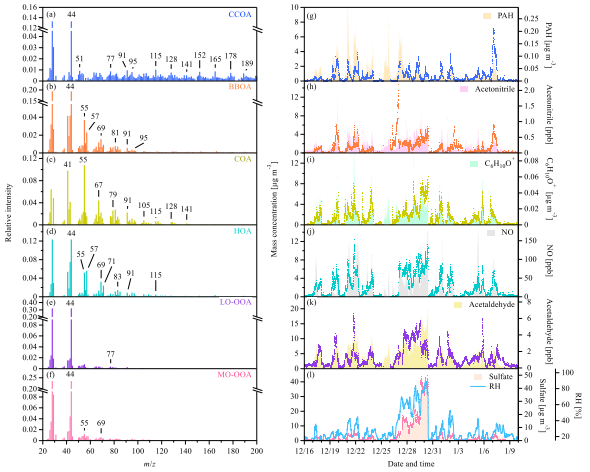

Figure S5. (a-f) Mass spectra and (g-l) time-series of the six OA factors (CCOA, BBOA, COA, HOA, LO-OOA, MO-OOA) resolved from the PMF analysis.

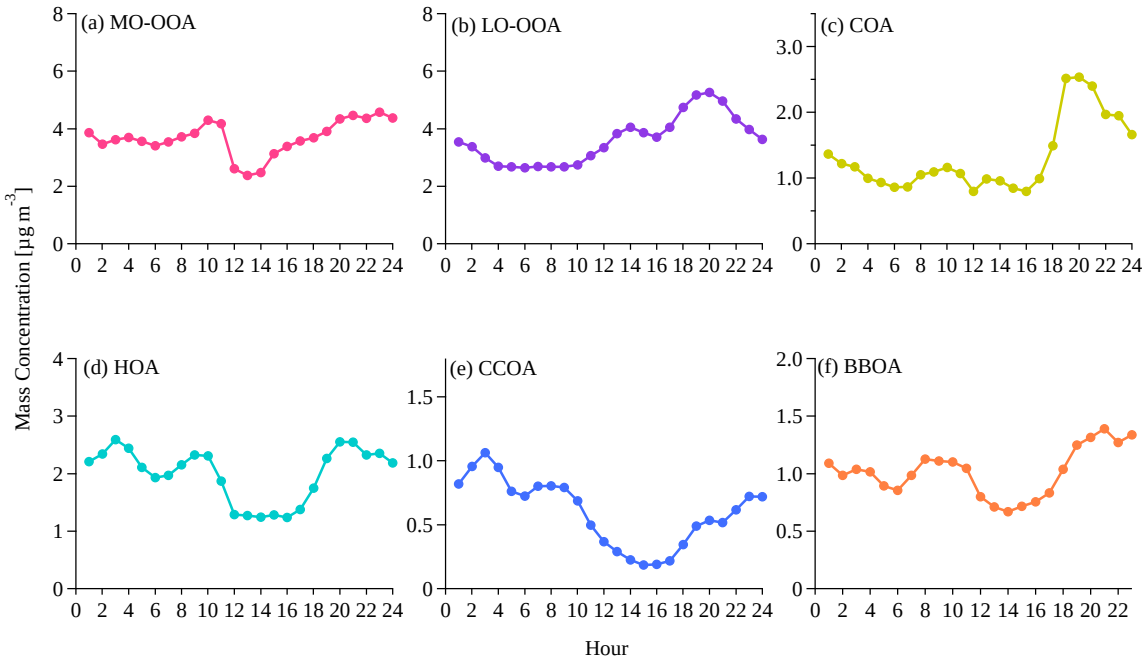

Figure S6. Diurnal patterns of the mean mass concentration of each statistical PMF factors of OA.

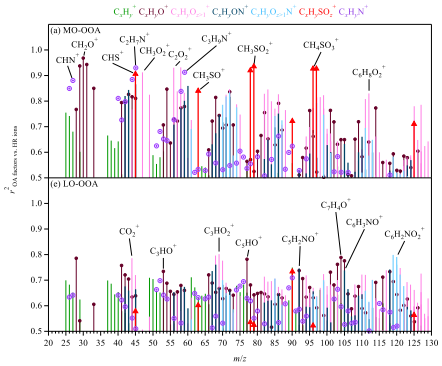

Figure S7. Correlations between two SOAs (MO-OOA and LO-OOA from the ACSM) and the HRMS ions from the AMS. The ions are categorized into 7 groups marked by different colors ($C_xH_y^+$, $C_xH_yO^+$, $C_xH_yO_{z>1}^+$, $C_xH_yON^+$, $C_xH_yO_{z>1}N^+$, $C_xH_ySO_z^+$, $C_xH_yN^+$).

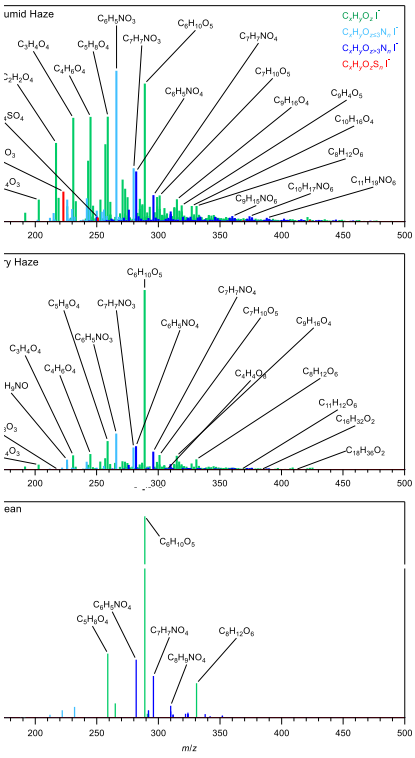

Figure S8. The averaged high-resolution mass spectra of CHOX compounds of the filter samples for (a) humid-haze day (YY/MM/DD, 17/12/29), (b) dry-haze day (17/12/21), and (c) clean day (17/12/22) obtained by the I^--TOF-CIMS with a FIGAERO. The ion signals are normalized to the signals of reagent ion I^-. Formulas stand for the corresponding molecules of the ions and are categorized into different family groups.

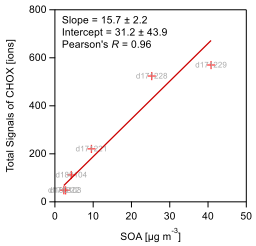

Figure S9. Comparisons between the total signal intensities of the selected 1881 $C_xH_yO_zX_n$ ions that are clustered with I^- and the OOA mass concentration of $PM_{2.5}$ for the six days. The fitted red line represents the orthogonal distance regression with an intercept.

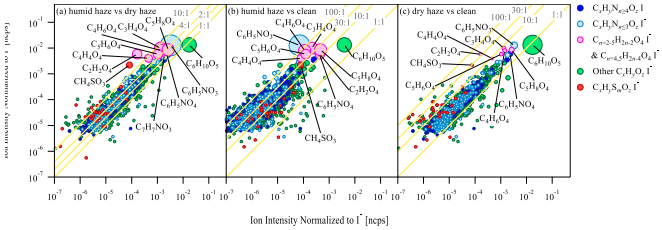

Figure S10. Comparisons of the averaged mass spectra between (a) humid haze and dry haze, (b) humid haze and clean days, (c) dry haze and clean days. The ion intensities are normalized to the intensity of I^-. The marker are colored by different groups and sized by the normalized total signal intensities of each ion during the humid haze or dry haze.

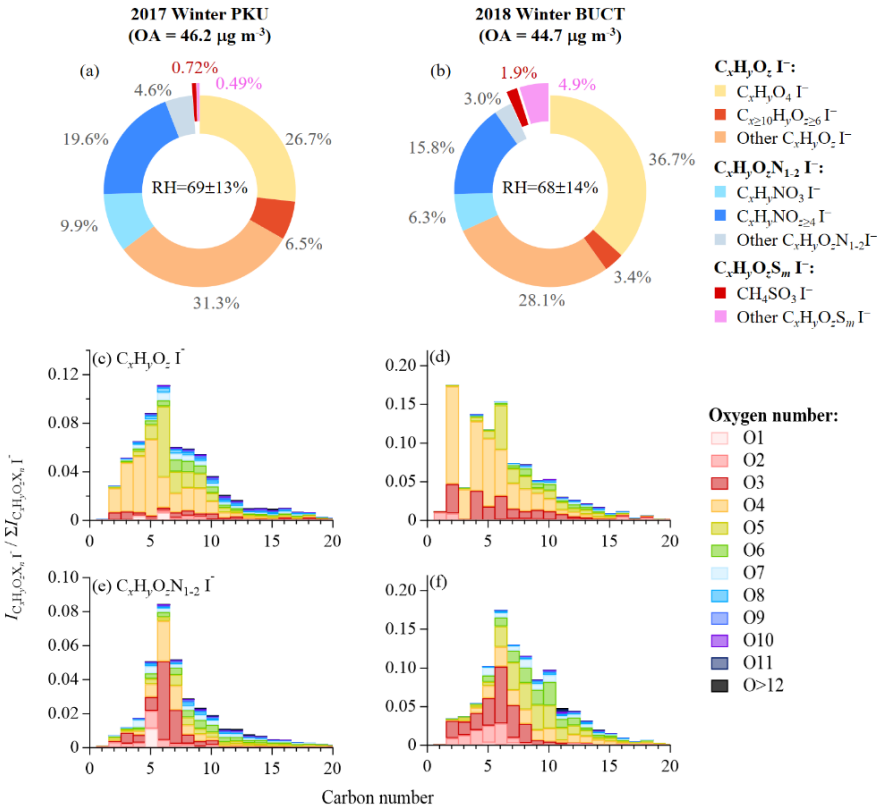

Figure S11. Signal intensity fraction of $C_xH_yO_z$, $C_xH_yO_zN_n$, and $C_xH_yO_zS_n$ compounds that cluster with I^- and stacked relative intensities of $C_xH_yO_z \cdot I^-$ and $C_xH_yO_zN_n \cdot I^-$ ions that are classified by carbon and oxygen numbers in their formulas for different humid-haze periods in Beijing during (a, c, e) 2017 winter (this study) and (b, d, f) 2018 autumn (Cai et al., 2021). These two measurements were performed in two laboratories using different I^- CIMS.

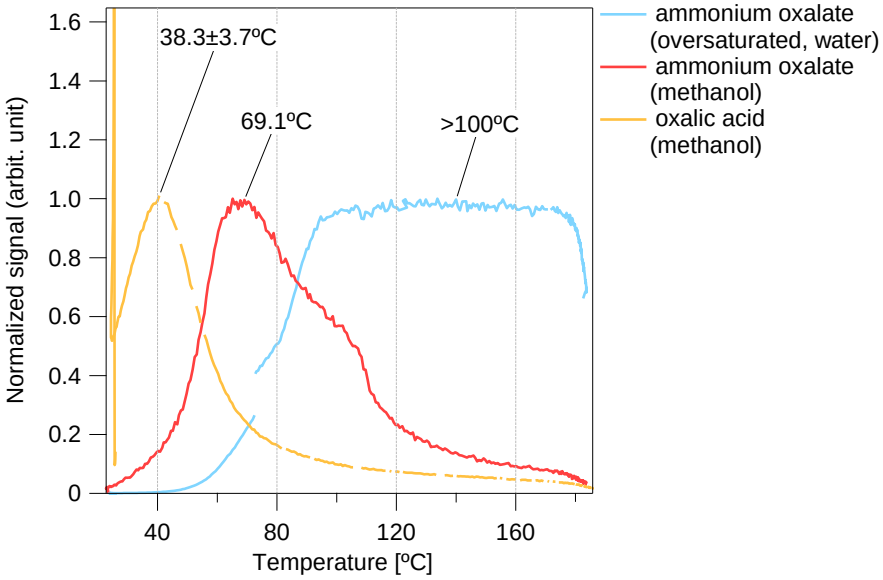

Figure S12. Thermograms of oxalic acid and ammonium oxalate measured in the laboratory.

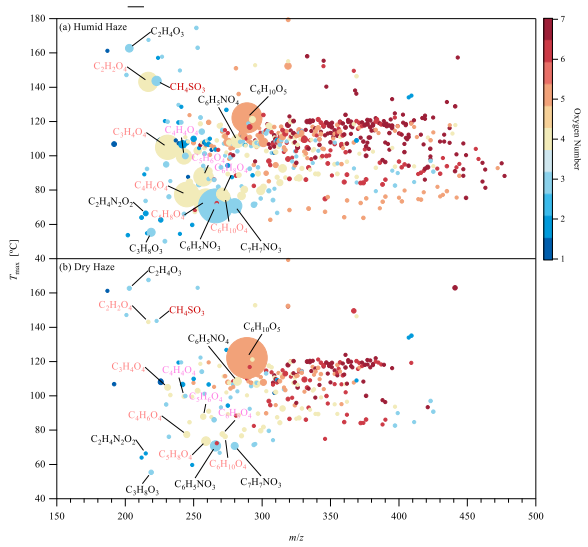

Figure S13. Distribution of mean T_{max} for $C_xH_yO_zX_n$ compounds as a function of m/z (including iodide, 126.9050 Th) for (a) humid haze and (b) dry haze. The $C_xH_yO_zX_n$ here include $C_xH_yO_z$, $C_xH_yO_zN_n$, and $C_xH_yO_zS_n$ compounds that cluster with I^-. The values of T_{max} are obtained from the averaged $\underline{T}_{max}$ from the humid haze with the standard deviation around 1.5~14.2°C (10th and 90th percentiles). The markers are colored by the oxygen number of each compound and sized by the signal at same scale for the two periods. Compounds with the intensity less than 0.5% of the strongest ion during the humid haze ($C_6H_5NO_3$ I^-) are omitted for clarity. In total 602 compounds during the humid haze and 296 compounds during the dry haze are presented here.

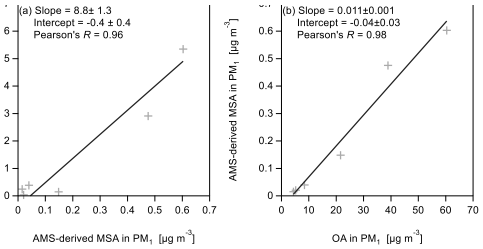

Figure S14. (a) Correlations between the normalized total signal intensities of CH_4SO_3 I^- obtained by the FIGAERO I^--ToF-CIMS and the AMS-derived methanesulfonic acid (MSA) mass concentrations on the basis of the $CH_3SO_2^+$ signals. (b) Correlations between the mass concentrations of AMS-derived MSA and OA for submicron particles (PM_1).

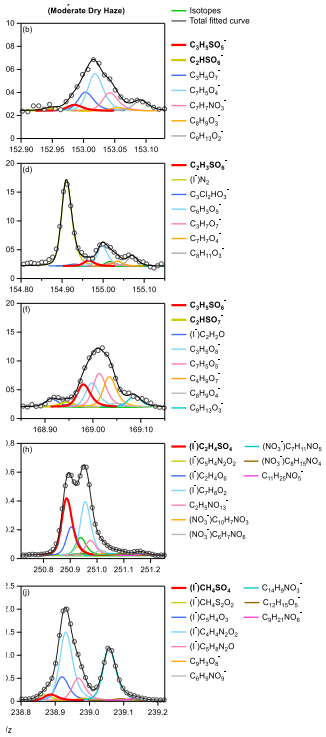

Figure S15. The high-resolution peak fitting at for major sulfur-containing oxygenated compounds during the severe humid haze (left) and moderate dry haze (right), including four types of organosulfates (a, b) $C_3H_5SO_5^-$, (c, d) $C_2H_3SO_6^-$, (e, f) $C_3H_5SO_6^-$, (g, h) $(I^-)C_2H_4SO_4$, and hydroxymethanesulfonic acid (HMSA) (i, j) $(I^-)CH_4SO_4$. The mass spectra are period-averaged.

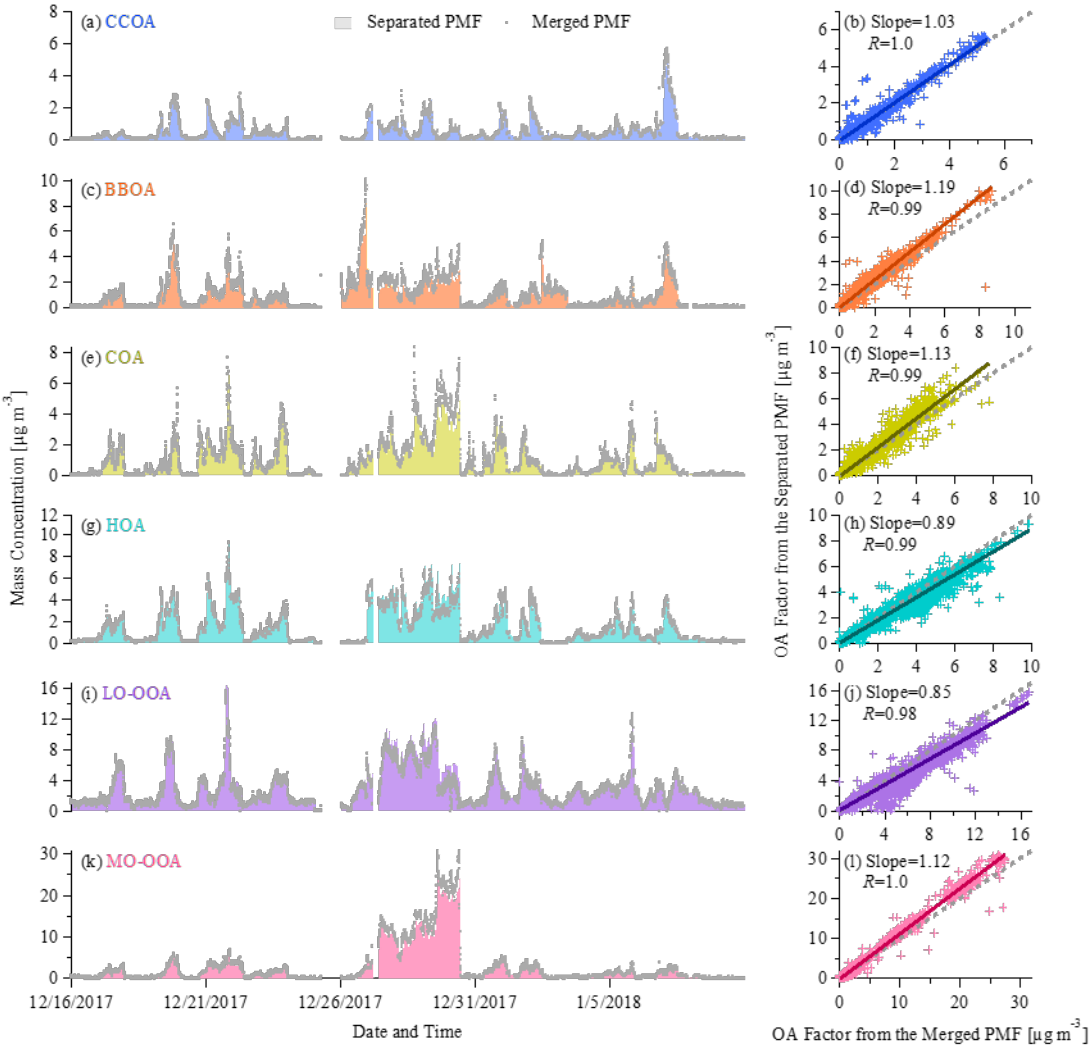

Figure S16. Comparisons of PMF results from separated-PMF and merged-PMF from the ACSM data (PM_1). The thick lines in the scatter plot are the orthogonal distance regression with intercept and the grey dashed lines refer to the 1:1 line for reference. The slopes and the Pearson's *R* are shown.

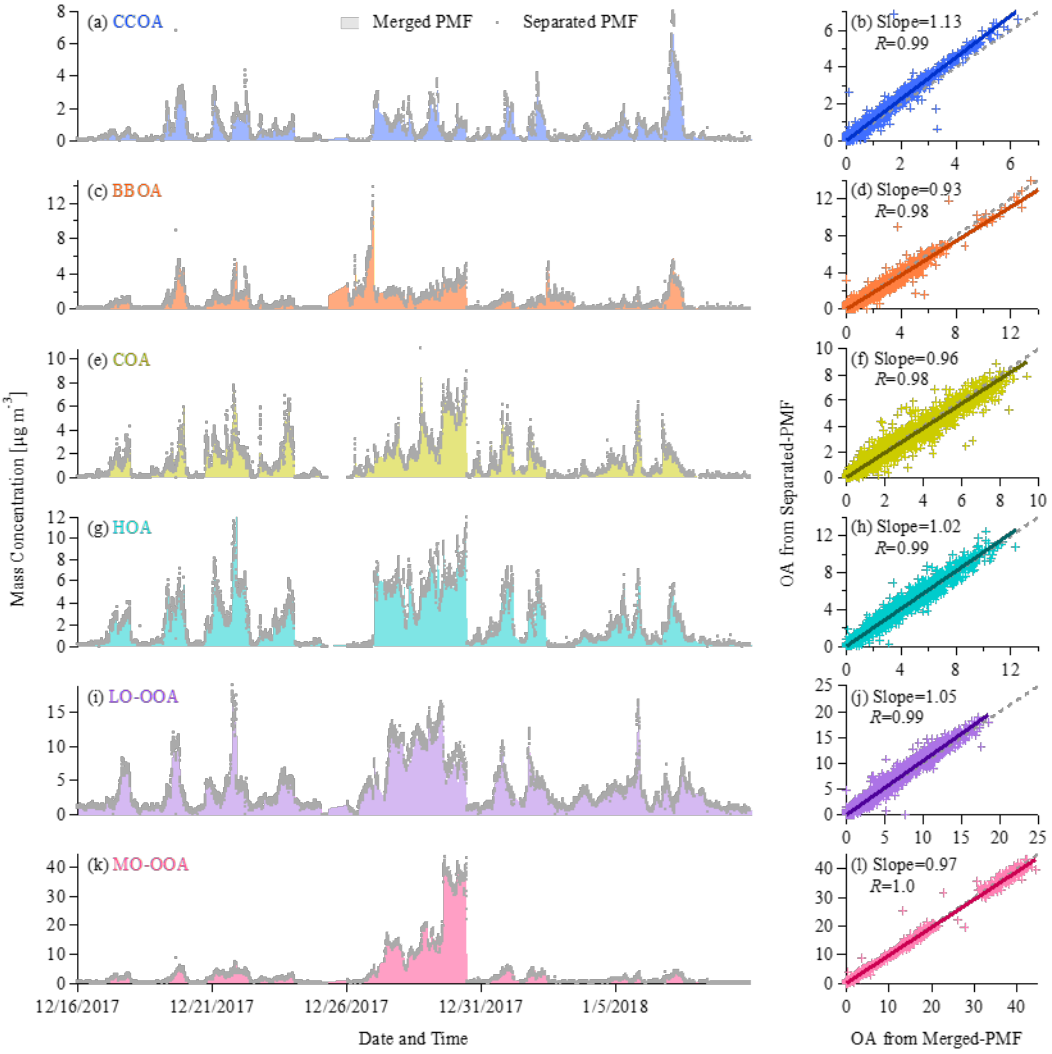

Figure S17. Comparisons of PMF results from separated-PMF and merged-PMF from the ACSM data ($PM_{2.5}$). The thick lines in the scatter plot are the orthogonal distance regression with intercept and the grey dashed lines refer to the 1:1 line for reference. The slopes and the Pearson's *R* are shown.

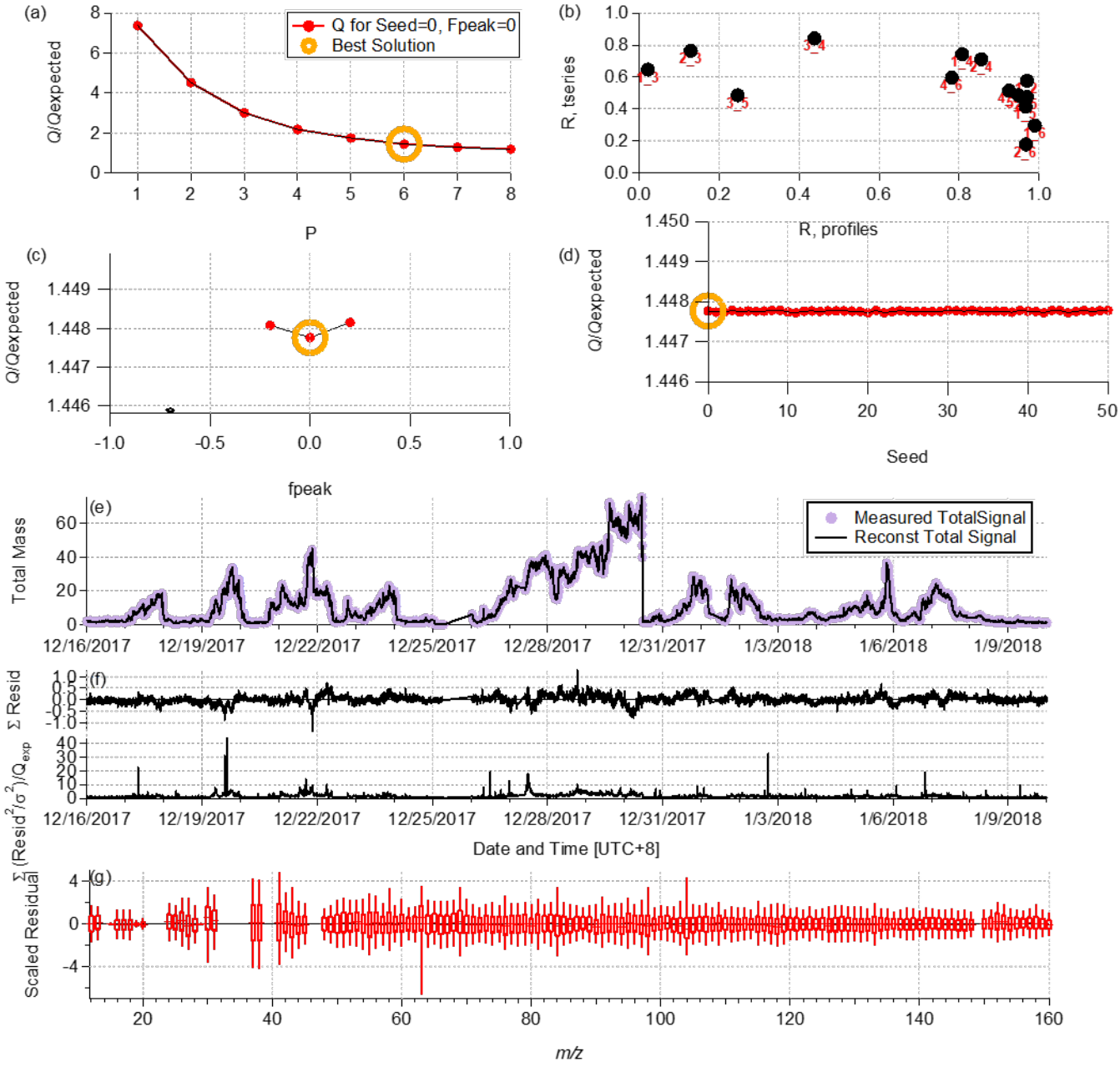

Figure S18. Diagnostics plots of PMF selection for $PM_{2.5}$ in Beijing, 2017 winter (CV-ACSM).

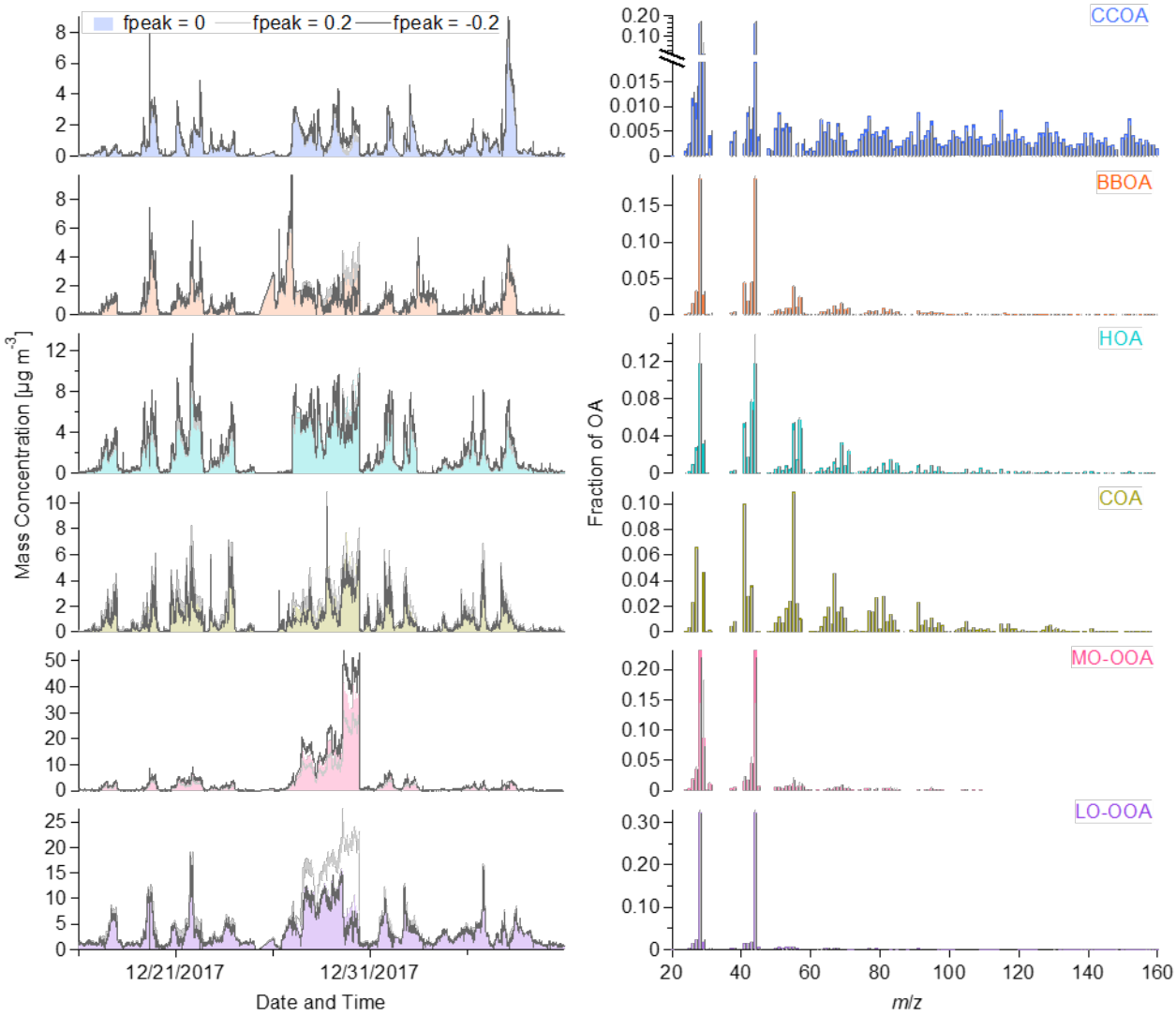

Figure S19. Diagnostics plots of PMF selection for $PM_{2.5}$ in Beijing, 2017 winter (CV-ACSM) The mass spectra and time-series of the 6-factor solution at different fpeak values.

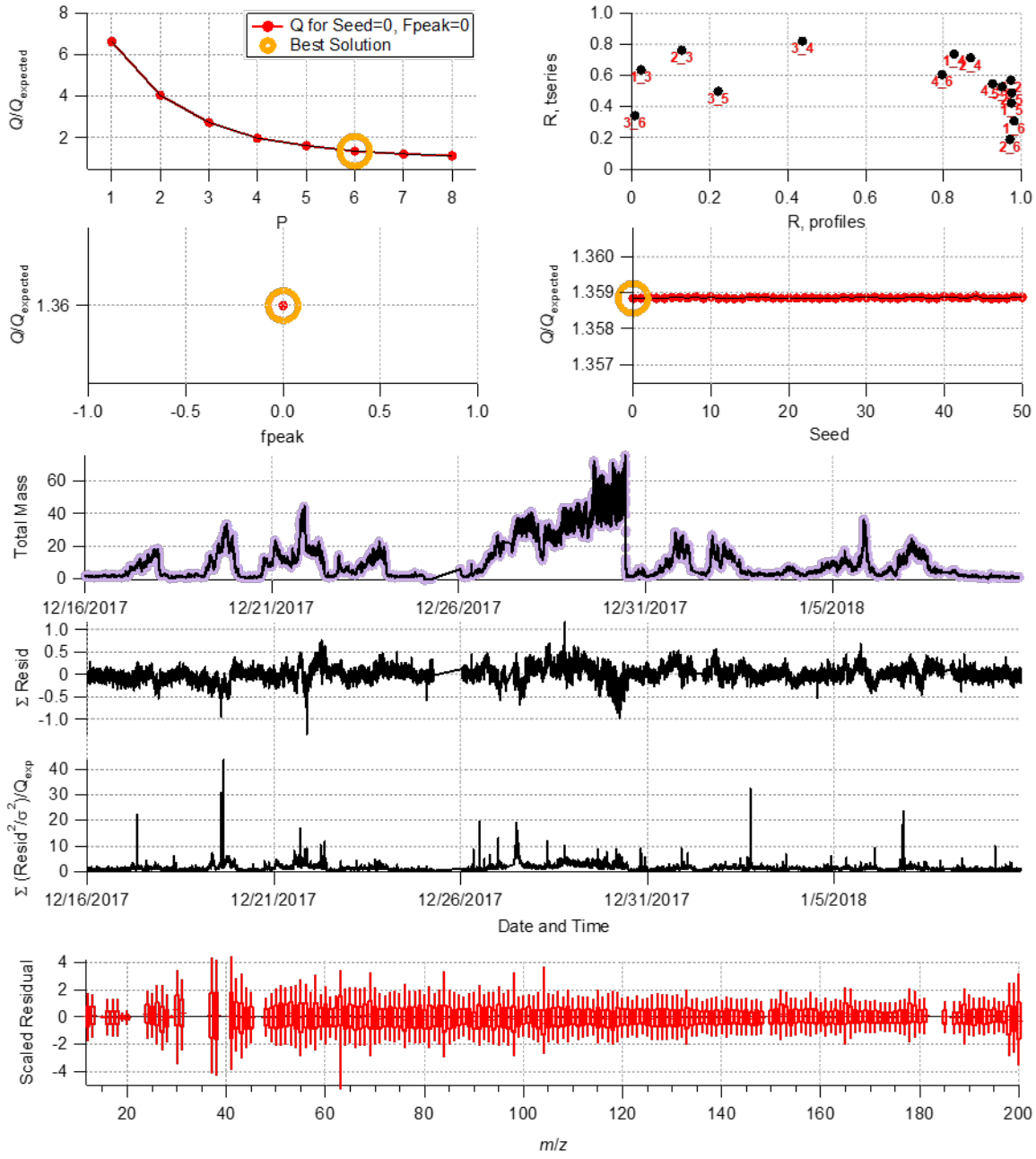

Figure S20. Diagnostics plots of PMF selection for the PM_1-$PM_{2.5}$ merged datasets in Beijing, 2017 winter.

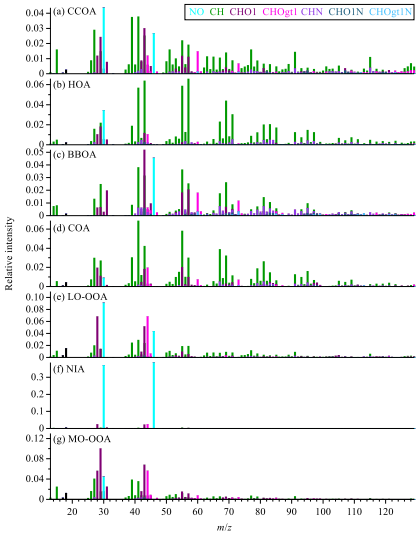

Figure S21. Mass spectra of the NIA factor and six OA factors (CCOA, HOA, BBOA, COA, LO-OOA, and MO-OOA) that are identified from the organic-inorganic mixed PMF analysis based on the AMS data (PM_1).

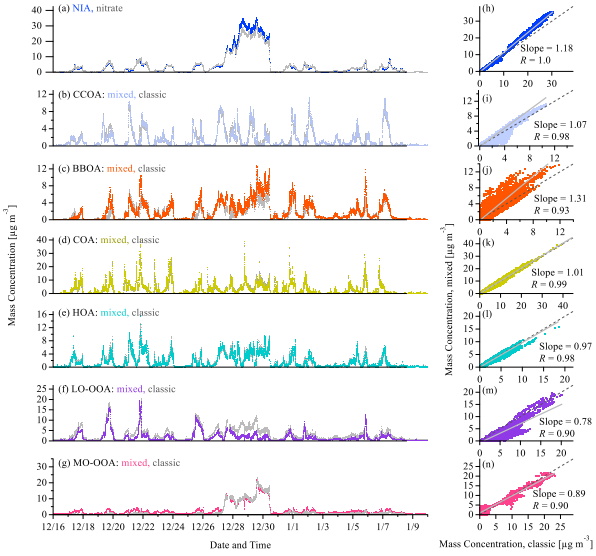

Figure S22. Comparisons of the time-series of the NIA factor and the six OA factors based on the organic-inorganic mixed PMF method with the results from the classic PMF method.

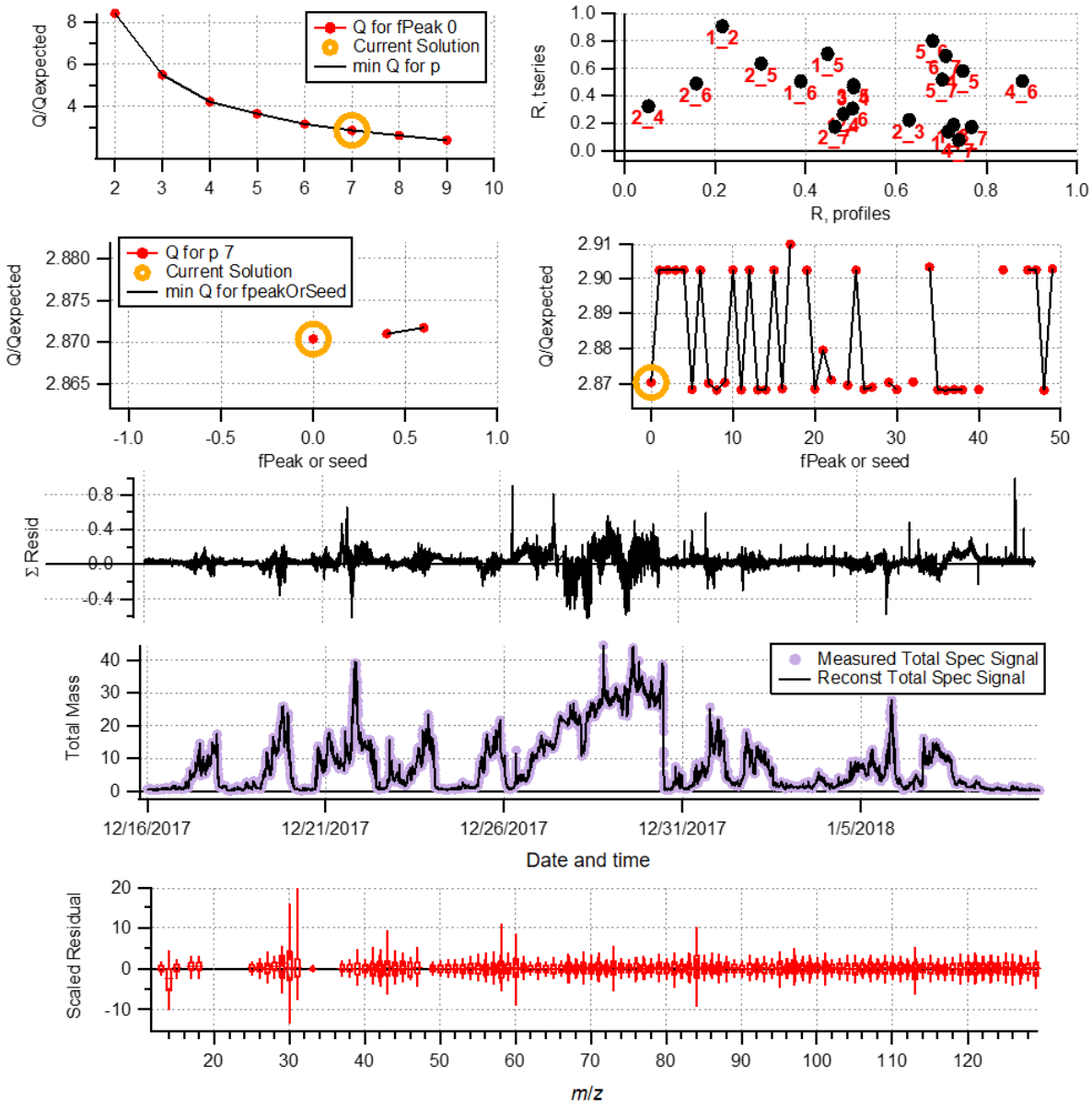

Figure S23. Diagnostics plots of PMF selection for the organic-inorganic mixed datasets from AMS.

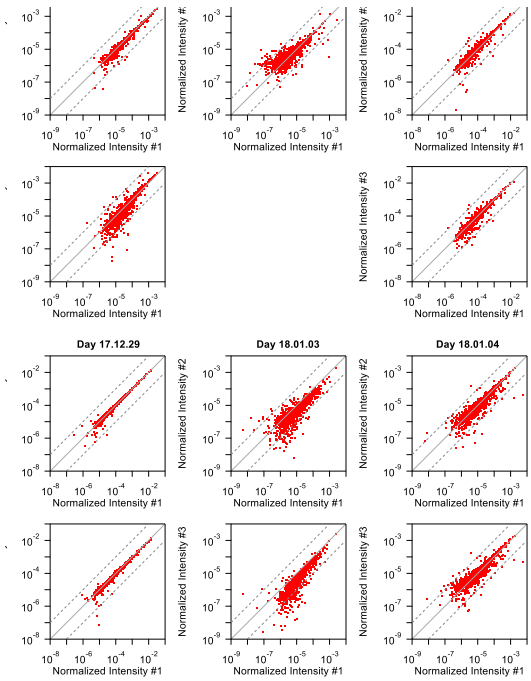

Figure S24. Comparisons of the mass spectra from the parallel samples of each day. For the day 2017.12.22, only 2 parallel samples are available.